Title: p16-dependent increase of PD-L1 stability regulates immunosurveillance of senescent cells

Authors: Julia Majewska[*1†], Amit Agrawal[1†], Avi Mayo[1], Lior Roitman[1], Rishita Chatterjee[2], Jarmila Kralova[2], Tomer Landsberger[3], Yonatan Katzenelenbogen[3], Tomer Meir-Salame[4], Efrat Hagai[4], Ilanit Sopher[1], Juan-Felipe Perez-Correa[5,6], Wolfgang Wagner[5,6], Avi Maimon[1], Ido Amit[3], Uri Alon[1] Valery Krizhanovsky[*1]

Affiliations:

[1]Department of Molecular Cell Biology, Weizmann Institute of Science; Rehovot, 7610001, Israel

[2]Department of Immunology and Regenerative Biology, Weizmann Institute of Science; Rehovot, 7610001, Israel

[3]Department of Systems Immunology, Weizmann Institute of Science; Rehovot, 7610001, Israel

[4]Department of Biological Services, Weizmann Institute of Science; Rehovot, 7610001, Israel

[5]Institute for Stem Cell Biology, RWTH Aachen University Medical School, Aachen Germany

[6]Helmholtz Institute for Biomedical Engineering, RWTH Aachen University Medical School, Aachen Germany

[†] These authors contributed equally to this work

[*]Corresponding authors. Email: julia.majewska@weizmann.ac.il, valery.krizhanovsky@weizmann.ac.il

Abstract: The accumulation of senescent cells promotes aging and age-related diseases, but molecular mechanisms that senescent cells use to evade immune clearance and accumulate in tissues remain to be elucidated. Here, we report that p16-positive senescent cells upregulate the immune checkpoint protein programmed death-ligand 1 (PD-L1) to accumulate in aging and chronic inflammation. We show that p16-mediated inhibition of cell cycle kinases CDK4/6 induces PD-L1 stability in senescent cells via downregulation of its ubiquitin-dependent degradation. p16-expressing senescent alveolar macrophages elevate PD-L1 to promote an immunosuppressive environment that can contribute to an increased burden of senescent cells. Treatment with activating anti-PD-L1 antibodies engaging Fcγ receptors on effector cells leads to the elimination of PD-L1 and p16-positive cells. Our study uncovers a molecular mechanism of p16-dependent regulation of PD-L1 protein stability in senescent cells and reveals the potential of targeting PD-L1 to improve immunosurveillance of senescent cells and ameliorate senescence-associated inflammation.

Main text:

Introduction

Senescent cells accumulate in tissues with age, disrupt tissue homeostasis, promote aging, and limit lifespan (*1*). Conversely, the elimination of senescent cells significantly delays the onset of age-related phenotypes including age-associated inflammation (inflammaging), and extends lifespan in animal models (*2, 3*). However, the therapeutic potential of senolytic drugs that could selectively clear senescent cells is hampered due to their insufficient specificity and toxicity (*4*). Understanding the molecular basis underlying the impaired immunosurveillance of senescent cells, and thus allowing their presence in aging tissues could provide strategies regulating senescent cell turnover and ameliorating senescence-associated phenotypes.

The age-dependent decline of immune-mediated clearance of senescent cells depends on senescent cell-autonomous mechanisms that inhibit their removal (*5, 6*), and functional impairment of the aged immune system (immunosenescence) (*7, 8*). Still, the intrinsic properties of senescent cells limiting their immunosurveillance and mechanisms explaining the immunosenescence-associated increased senescent cell burden in aging and diseased tissues remain to be elucidated.

In the present study, we used mass cytometry to study senescent cell accumulation in aging and chronically inflamed lungs in mice. We found that p16-positive senescent cells upregulate PD-L1 to evade immunosurveillance and accumulate in aging and chronic inflammation. Our study reveals the molecular mechanism that regulates PD-L1 stability in senescent cells. p16-mediated inhibition of cyclin-dependent kinases (CDK)4/6 downregulates ubiquitin-dependent proteasomal degradation of PD-L1 leading to its accumulation in senescent cells. Moreover, sequencing of p16-expressing alveolar macrophages in chronic lung inflammation has revealed a transcriptional immunosuppressive signature coupled to p16 expression. We show that activating PD-L1 antibody engaging Fcγ receptors on effector cells enhances immune-mediated clearance of senescent cells *in vivo*. Consistent with this, the administration of these activating PD-L1 antibodies to naturally aging mice and mice with chronically inflamed lungs reduces p16, PD-L1 double-positive senescent cells, and ameliorates senescence-associated inflammation.

Results

p16-positive senescent cells upregulate immune checkpoint PD-L1 in aging and chronic inflammation

Immunosenescence has a causal role in driving systemic aging, including an increased burden of senescent cells (*7*). To unravel cell-autonomous mechanisms leading to impaired immunosurveillance of senescent cells, we investigated functional phenotypes of immune cells undergoing senescence with age. We performed a mass cytometry analysis on lung immune cells from young 2-month- and aged

24-month-old C57BL/6 wild type mice. viSNE analysis of the $CD45^+$ immune cells distinguished alveolar and interstitial macrophages (AM and IM respectively), natural killer (NK) cells, eosinophils, neutrophils, $CD4^+$ and cytotoxic $CD8^+$ T cells, and $CD11b^+CD11c^+$ myeloid cells (Fig. 1a, Extended Data Fig. 1a). In aged lungs, the frequencies of AM and $CD11b^+CD11c^+$ myeloid cells were significantly increased, both the relative and absolute cell numbers (Fig. 1b, Extended Data Fig. 1b-c). We then analysed each of the identified immune cell types for the expression of senescence-related proteins. Remarkably, AMs were particularly enriched for senescence (p16, p21), pro-inflammatory (p-p38, p-p65), and immunoregulatory (MHCI) markers in aged mice compared to young counterparts (Fig. 1c). Strikingly, AM also showed the highest expression of immune checkpoint molecule PD-L1 protein comparing to all other immune subsets (Fig. 1d). Of note, AMs showed a significantly increased level of PD-L1 as a function of p16 expression, which was further pronounced in aging (Fig. 1e-f). Single-cell analysis of AM revealed a positive correlation between p16 and PD-L1 (Spearman's rank correlation coefficient young - 0.9, old – 0.9; Fig. 1f). We then wanted to understand if p16 expression is coupled with the other proteins related to the senescent phenotype. We analysed fold change of expression of senescence-related proteins as a function of p16 level and found that cyclin-dependent kinase inhibitor p21 (Cdkn1a), anti-apoptotic protein BCL-XL, and MHCI showed the most striking correlation with p16, irrespective of the age of mice (Fig. 1g). Increased expression of p21 and BCL-XL is known to underlie senescent cells' resistance to apoptosis and can contribute to their accumulation in tissues (*9, 10*). To understand if the observed phenomena is not limited to AM, we analysed lung epithelium, which is known to accumulate senescent cells in the aging (*11, 12*). Similarly, to AM, epithelial cells showed significant upregulation of PD-L1 expression as a function of p16 expression in both, young and old mice, but again with higher levels in old mice (Spearman's rank correlation coefficient: young – 0.73, old - 0.86; Fig. 1h-i). We found that expression of core proteins of the senescence machinery (p21, p53), followed by proteins involved in inflammatory response (p-p65, p-p38) showed the strongest correlation with p16 level, regardless of age (Fig. 1j). These results indicate that the expression of p16 is correlated with PD-L1 expression in senescent cells, with higher levels of expression of both proteins in older mice (Fig. 1e-f, h-i). We hypothesized that macrophages with senescent phenotype might contribute to inflammation, but also induce a compensatory immunosuppressive response to prevent excessive tissue damage. This is in agreement with a recently reported subset of p16-expressing AMs with senescence-like properties in aging lungs, which suppress cytotoxic T-cell responses (*13*). Thus, in aging, increased expression of p16 associated with PD-L1-mediated immunosuppression might lead to compromised immunosurveillance and consequently increased senescent cell burden.

Previously, we have reported that accumulating senescent lung epithelial cells promote chronic lung inflammation (*14*). We therefore asked if p16-positive senescent cells upregulate PD-L1 in chronically inflamed lungs, which might explain their compromised immune clearance. To address this question,

we used a mouse model of LPS-induced chronic lung inflammation, which resembles the pathology of chronic obstructive pulmonary disease (COPD) (*15*). To comprehensively characterize senescence in the epithelium, we took an unbiased mathematical approach to study cellular and phenotypic diversity of p16-positive senescent cells within the non-immune, non-endothelial cell compartment ($CD45^-$ $CD31^-$) in chronic lung inflammation by mass cytometry. Principal component analysis (PCA) of the data identified three distinct clusters (designated as clusters 1, 2, and 3) within this cell population derived from inflamed (LPS, Infl) and control (PBS, Ctrl) lungs (Fig. 2a, Extended Data Fig. 2a). Density of cells within cluster 1, but not the other two clusters, significantly increased upon chronic inflammation (Fig. 2b). Cells within cluster 1 were significantly enriched in the expression of epithelial marker EpCam, and other canonical markers of lung epithelium subsets (SPC/SPB – alveolar cell type II, HOPX/PDPN – alveolar cell type I, CC10 – club cells; Muc5AC – goblet cells; KRT5/KRT14 – basal cells; KRT8 - alveolar progenitor cells, Fig. 2c, left, Extended Data Fig. 2b), indicating their epithelial identity. Cells in cluster 2 showed expression of the basal progenitor marker KRT14 (Extended Data Fig. 2b), and cluster 3 was enriched in fibroblast markers (CD90.2, CD140a, CD140b) (Fig. 2c, right). Analysis of senescence markers in cells of cluster 1 showed enrichment for proteins of cell cycle arrest (p16, p21, p53), and depletion of the proliferation marker Ki-67 (Fig. 2d). Cells in cluster 1 were also enriched for molecules involved in the pro-inflammatory pathways (p-p38, p-p65, CD54), which can promote chronic inflammation (Fig. 2d). Remarkably, cells in cluster 1 also upregulated molecules associated with antigen presentation (MHCI, MHCII) and the immune checkpoint molecule PD-L1 (Fig. 2e), similar to what we observed in the lungs of old mice. These results suggest that p16-positive senescent cells with enhanced MHC machinery express PD-L1, thus providing an intrinsic mechanism for their escape from immunosurveillance, and explaining their role in chronic inflammation by dysregulating immune responses.

Our next aim was to further understand how epithelial cells mediate the dysregulation of immune responses upon chronic damage. To address this, we performed RNA-sequencing of purified lung epithelial cells from LPS-treated and control mice. Gene ontology (GO) enrichment analysis of genes upregulated in the lung epithelium of mice with chronic inflammation indicated a marked increase in the expression of genes involved in a pro-inflammatory response, antigen processing, and presentation (Extended Data Fig. 2c-d). Furthermore, we observed an increase in gene signatures related to the activation of adaptive and innate immune responses, suggesting that the epithelial compartment enriched with senescence enhances the activation of macrophages during chronic inflammation.

We further hypothesized that chronic inflammation might promote immune cells to undergo senescence, which in turn comprises immune cell function and results in the higher burden of damaged, or senescent cells. We evaluated immune cell populations using a senescence and immune-cell-centric antibody panel. viSNE analysis performed on $CD45^+$ immune cells distinguished AM, IM, NK cells, eosinophils, neutrophils, $CD4^+$ and $CD8^+$ T cells, B cells, and $CD11b^+Ly6C^+$ myeloid cells (Fig. 2f,

Extended Data Fig. 2e). In chronically inflamed lungs, we observed a significant increase in AM and IM (Fig. 2g). We analysed all the identified immune cell populations for the expression of senescence-related proteins. Only AM and IM were enriched for the expression of senescence (p16, p21), pro-inflammatory (p-p38), and immunoregulatory (MHCI) markers in chronically inflamed compared to control mice (Fig. 2h; Extended Data Fig. 2f-g). The macrophages also showed the highest expression of PD-L1 protein compared to all other immune subsets, both in steady state and during inflammation (Fig. 2i). However, the mean expression levels of p16 and PD-L1 were higher in alveolar than in interstitial macrophages (Fig. 2j). Of note, the expression of p16 in AM was significantly correlated with PD-L1 levels, consistent with our observation of age-related changes in AM (Spearman's rank correlation coefficient LPS - 0.71, PBS – 0.76; Fig. 2k-l). Together, these results show that chronic inflammation triggered the accumulation of macrophages with a senescent phenotype and induced the expression of PD-L1 in these cells.

Alveolar macrophages and the epithelial lining of the respiratory tract are the first lines of cellular and physical defence against environmental hazards such as cigarette smoke, allergens, and other air-born pollutants (*16, 17*). Pulmonary epithelium also interacts with immune cells to maintain homeostasis while facilitating immune response when necessary (*16*). Senescence of lung epithelium promotes chronic lung inflammation (*14*), and upregulation of PD-L1 in both senescent epithelial cells and macrophages with senescent phenotype might be an intrinsic mechanism to evade immune clearance and promote persistent senescence in the tissue. We suggest that the upregulation of immune checkpoint PD-L1 on damage-induced senescent cells minimizes autoreactive immune responses in chronic inflammation to preserve organ integrity and function.

p16-mediated inhibition of CDK4/6 links decreased ubiquitination to the upregulation of PD-L1 stability in senescence

To explore the molecular mechanism behind the elevation of PD-L1 in senescent cells, we used a classical model of cellular senescence in primary mouse (Ccl206) and human (IMR90) lung fibroblasts induced to senesce by DNA damage (*10*). Senescence induction significantly increased surface PD-L1 expression compared to growing control cells (Fig. 3a-b, Extended Data Fig. 3a). Replicative exhaustion, another physiological inducer of senescence, also caused PD-L1 upregulation (Fig. 3b, Extended Data Fig. 3a). An overexpression of p16 induced elevation of PD-L1 protein levels in mouse, but not in human cells (Fig. 3c, Extended Data Fig. 3b-c). Under *in vitro* culture conditions, mouse cells accumulate DNA damage faster than human cells, which might explain interspecies differences in p16 overexpression and change in PD-L1 level. Interestingly, cells induced to senesce by overexpression of p16 (and without induced DNA damage), don't express SASP components despite other hallmarks of senescence (*18*). These results suggest that regardless of the species, DNA-damage-mediated senescence-associated inflammation plays a key role in the regulation of PD-L1 expression with p16 further promoting its increased protein levels.

p16 inhibits cyclin-dependent kinases (CDKs)4/6 to induce proliferative arrest in senescent cells. To test if PD-L1 upregulation is enhanced by p16-mediated inhibition of CDKs, we treated growing primary fibroblasts with highly selective inhibitors of CDK4 and CDK6 (CDK4/6i), abemaciclib or palbociclib, which can be considered functional p16 mimetics (*19*). Treatment with CDK4/6i significantly elevated surface PD-L1 expression (Fig. 3d-e). To understand whether the observed increase of PD-L1 protein in senescent cells is mediated by p16-dependent inhibition of CDK4/6, we silenced gene encoding p16 (Cdkn2a) in senescent cells. We found that this knockdown efficiently reduced PD-L1 protein levels in senescent cells (Fig. 3f). Since inhibition of proteasomal-mediated degradation induces stability of many proteins to ensure cellular integrity in response to stress (*20*), we hypothesized that this mechanism might be responsible for p16-mediated PD-L1 upregulation. To examine the effect of p16 on the stability of endogenous PD-L1 protein in senescent IMR90 cells, we used a cycloheximide (CHX) chase assay to block translation and measure the degradation rate of PD-L1 protein. Knockdown of p16 caused a significant acceleration of PD-L1 turnover three hours post CHX treatment (Fig. 3g), indicating that PD-L1 degradation is p16-dependent. These results demonstrate that p16-mediated inhibition of CDK4/6 promotes PD-L1 protein stability in cellular senescence.

E3 ubiquitin ligases control PD-L1 protein levels through ubiquitin-dependent proteasomal-mediated protein degradation (*21*). SCF (SKP1-CUL1-F-box protein) E3 ubiquitin ligases constitute the largest family responsible for the turnover of key regulatory proteins of the cell cycle (*22*). β-TrCP is a substrate recognition component of SCF complex, also known to mediate PD-L1 ubiquitination for subsequent degradation (*21*). We reasoned that in cellular senescence the activity of SCF might be altered, thus affecting PD-L1 ubiquitination. We found that β-TrCP levels in senescent cells are downregulated compared to growing control cells (Fig. 3h), possibly contributing to elevated PD-L1 levels in senescence (Fig. 3h). Depletion of p16 in senescent cells restored β-TrCP level, possibly explaining the accelerated degradation of PD-L1 in senescent cells with p16 knockdown (Fig. 3g, i, Extended Data Fig. 3d). Given that SCF ubiquitin ligase governs the ubiquitination and degradation of PD-L1 via β-TrCP, we evaluated its ubiquitination levels in senescent cells. Immunoprecipitation of PD-L1 indicated a significantly lower ubiquitination signal in senescent cells compared to growing (Fig. 3j). Treatment with the proteasome inhibitor MG132 showed a trend of PD-L1 protein increase in growing cells but did not affect PD-L1 levels in senescent cells, further indicating a reduced proteasomal degradation of PD-L1 in senescent cells (Fig. 3k). These results indicate that p16 in senescence is linked to the upregulation of PD-L1 stability via decreased proteasome-mediated degradation.

Multiple mechanisms regulate PD-L1 at the transcriptional, posttranscriptional, and posttranslational levels (*23*). The pro-inflammatory secretome of senescent cells can upregulate PD-L1 mRNA expression through the JAK-STAT pathway (*24*). In cancer cells, cyclin D-CDK4/6 dependent

phosphorylation of SPOP/Cullin-3 ubiquitin ligase complex destabilizes PD-L1 via proteasome-mediated degradation, but inhibition of CDK4/6 significantly elevates PD-L1 level (*25*). Interestingly, in tumor cells the expression of p16 strongly correlates with PD-L1 levels, highlighting the therapeutic potential of PD1-PD-L1 immune checkpoint therapy (*25, 26*). Similarly, in lung adenocarcinoma and squamous cell carcinoma patients, we observed a significant accumulation of cells expressing both p16 and PD-L1 (Fig. 3l, Extended Data Fig. 3d). Furthermore, in patients with emphysema, a tissue manifestation of COPD, and lung fibrosis, we also identified p16, PD-L1 double-positive cells (Fig. 3l-m, Extended Data Fig. 3d). This data suggests that p16-positive cells that co-express PD-L1, which suppresses anti-tumor response, could also contribute to immune suppression in aging, including chronic lung disease. Together, our results link p16-mediated inhibition of CDK4/6 and compromised ubiquitination to the upregulation of PD-L1 stability, which could lead to potential strategies to enhance the immune response against PD-L1 in senescent cells.

p16-positive alveolar macrophages show immunosuppressive phenotype

We observed that cellular senescence triggers p16-mediated induction of PD-L1 in aging and chronic inflammation. So far, it is unknown if p16 expression contributes to compromised immune surveillance. Therefore, we decided to investigate the functional significance of p16-positive cells in this process, focusing on AM, as an example, due to their distinct accumulation in chronic lung inflammation (Fig. 2g, Fig. 4a). We used INs-Seq, a sequencing technology that combines intracellular labeling with transcriptomics to study p16-expressing cells (*27*). Gene set enrichment analysis revealed marked upregulation of central genes involved in extracellular matrix remodeling or the response to retinoic acid in p16 high-expressing alveolar macrophages (Fig. 4b). Remarkably, p16 expression was negatively correlated not only with the DNA replication but also with immune responses, including dendritic cell activation or chemokine secretion (Fig. 4b). Alveolar macrophages contribute to respiratory tolerance via retinoic acid-mediated induction of Foxp3 expression in naïve T cells (*28*). In this line, in chronically inflamed lungs, we observed a significant increase of Foxp3+ Tregs enriched with marked PD1 expression (Fig. 4c-d). Interestingly, Tregs secrete regulatory cytokines, such as IL-4, and IL-10, which can modulate anti-inflammatory macrophage phenotype suggesting the cross-regulation of the immune response (*28*). Together, these results suggest that high-level expression of p16 in alveolar macrophages induces an immunosuppressive environment with compromised immune responses and might lead to non-resolving inflammation upon chronic damage.

Anti-PD-L1, but not anti-PD1, antibody treatment depletes p16, PD-L1-positive cells in vivo

Given the p16-dependent upregulation of PD-L1 in senescent cells, we wondered whether PD-L1 can serve as an extracellular marker to target senescent cells for depletion *in vivo*. To address this, we established a short-term LPS-mediated lung injury model, which results in infiltration of p16, PD-L1-double positive immune cells in LPS-stimulated mice compared to PBS control (Extended Data Fig.

4a-e). Specifically, alveolar macrophages identified as $CD11c^+SiglecF^+$ cells were enriched for PD-L1 and p16 expression, concomitantly with our results in the models of chronic inflammation and aging (Extended Data Fig. 4b, e). These experiments indicate that in response to stress, induction of endogenous p16 *in vivo* is associated with elevation of PD-L1 independently of the time scale of injury or identity of cell type responding to challenge. p16-mediated upregulation of PD-L1 in senescent cells makes it a potential target for monoclonal antibodies to stimulate anti-senescence immunity. Immunomodulatory PD-L1 antibodies can act either as antagonists to block the immune checkpoint PD1-PD-L1 axis or as agonists to enhance the immune response against target cells by engaging other immune system components (*29*). Anti-PD-L1 antibodies engage activating Fcγ receptors on effector immune cells which augments their *in vivo* activity (activating PD-L1 antibodies), while anti-PD1 antibodies block the axis in Fcγ-independent manner (*30*). The treatment with activating anti-PD-L1 antibodies resulted in significant depletion of $CD45^+$ cells positive for p16 and PD-L1, including a marked reduction of $p16^+PD\text{-}L1^+$ cells within the AM population, relative to the mice treated with isotype-matched control antibody (Extended Data Fig. 4f-g). Immune checkpoint blockade of PD1-PD-L1 axis can stimulate effector functions of lymphocytes, mainly CD8 T cells. We tested if anti-PD-L1 antibody-mediated depletion of $p16^+PD\text{-}L1^+$ AM has a functional consequence for T cell activity. We decided to narrow the analysis of T cells to bronchioalveolar fluid, the functional lung compartment of AM. The activating anti-PD-L1 antibody treatment significantly increased the percentage of CD8 T cells showing expression of activation markers ICOS and PD1, known to be expressed during early T cell activation (Extended Data Fig. 4h). We have observed that anti-PD-L1 treatment also induced expression of *IFNγ* by CD8 T cells marking the activation of their effector function (Extended Data Fig. 4i) (*31*). Recently, it has been proposed that anti-PD1 improves senescence immunosurveillance in a CD8 T cell-dependent manner (*32*). Interestingly, our comparative study showed that only the treatment with agonist anti-PD-L1 antibody (and not antagonist anti-PD1 antibody) led to the depletion of $p16^+PD\text{-}L1^+$ cells in the inflamed lungs (Fig. 4e-f). This effect was accompanied by an increase of CD8 T cells showing expression of activation markers ICOS and CD44 following anti-PD-L1 but not anti-PD1 treatment (Fig. 4g). These results suggest that in inflamed lungs Fc-gamma-receptor-positive cells (neutrophils, NK cells, monocytes) might be important players in the immune surveillance of senescent cells, either by direct cytotoxicity or by stimulating the activity of CD8 T cells.

Anti-PD-L1 antibody treatment depletes p16, PD-L1-positive cells in aging and chronic lung inflammation

Given that senescent cells promote inflammation, we tested whether anti-PD-L1 could mediate the elimination of senescent cells and attenuate inflammaging and senescence-promoted inflammation in aging and chronic lung diseases. Activating anti-PD-L1 antibodies resulted in significant depletion of $CD45^+$ positive for p16 and PD-L1 in aged lungs, including a marked reduction of $p16^+$ and $p16^+PD\text{-}$

312 $L1^+$ cells within the AM population, relative to the mice treated with isotype-matched control antibody
313 (Fig. 5a-b, Extended Data Fig. 5a). It was accompanied by a significant increase of CD8 T cells showing
314 expression of activation markers CD25 and PD1, NK cells with marked upregulation of CD69, and
315 decreased plasma levels of inflammatory cytokines (Fig. 5c-d, Extended Data Fig. 5b-c). Also, in
316 chronic lung inflammation, we observed the anti-PD-L1-mediated depletion of $p16^+PD\text{-}L1^+$ cells within
317 the general immune $CD45^+$ and AM population (Fig. 5e-f), together with significant activation of CD8
318 T cells expressing PD1 (Extended Data Fig. 5d), and decreased expression of cell-cycle regulators and
319 pro-inflammatory SASP factors (Fig. 5g). To understand if anti-PD-L1 mediated treatment could
320 reverse age-dependent immunosenescence we checked epigenetic aging of the peripheral immune
321 system in the blood by DNA methylation clock. There was no difference in the prediction of
322 chronological age between aged mice treated with anti-PD-L1 antibodies and the isotype control
323 (Extended Data Fig. 5e). Interestingly, recent reports suggest a relative stability of immune system
324 dynamics in aging over a short time (*33*). In addition, anti-PD-L1-mediated depletion of senescent cells
325 did not improve the capacity of the respiratory system upon chronic lung inflammation (data not
326 shown). Collectively, our data suggests that anti-PD-L1 treatment improves immunosurveillance of
327 senescent cells in physiological aging and chronic lung inflammation and ameliorates senescence-
328 associated pro-inflammation. However, the elimination of senescent cells by PD-L1 immune
329 checkpoint blockade might not necessarily be a promising anti-aging therapy, due to a limited effect on
330 systemic age- and senescence-associated dysfunction *in vivo.*

331

332 **Discussion**

333 We show that senescent cells upregulate the stability of PD-L1 in a p16-dependent manner and
334 exploit the PD-1/PD-L1 signaling axis as a general mechanism to escape immune surveillance.
335 Accordingly, activating anti-PD-L1 antibodies enhances an immune response to deplete PD-L1-positive
336 senescent cells *in vivo* (Extended Data Fig. 5f). Our results reveal the p16-dependent molecular
337 mechanism that regulates PD-L1 stability in senescent cells. Specifically, p16-mediated inhibition of
338 CDK4/6 downregulates ubiquitin-dependent proteasomal degradation of PD-L1, leading to its
339 accumulation in senescent cells. p16-dependent upregulation of PD-L1 in senescent cells allows
340 targeting of PD-L1 to improve immunosurveillance of senescent cells. Our findings reveal that the
341 activating PD-L1 antibody engaging Fcγ receptors on effector cells reduces p16, PD-L1 double-positive
342 senescent cells *in vivo* and ameliorates senescence-associated inflammation.

343 Importantly, senescent cells are a heterogeneous population *in vivo* with differential expression of
344 p16 and PD-L1, which might affect their PD-L1-mediated immunosurveillance. This is supported by
345 our results showing that overexpression of p16 only moderately induces PD-L1 gene expression in
346 mouse, but not human cells, which could be explained by enhanced accumulation of DNA damage in

murine system *in vitro* (Fig. 3c, Extended Data Fig. 3b-c). PD-L1 expression is regulated by factors coupled with aging, including DNA-damage-mediated inflammation (*24, 32*). This explains why PD-L1 expression is enhanced in aging, with p16 further promoting increased protein levels. Our study also underscores the important role of PD-L1 in the dynamics of senescent cell accumulation in aging. Modeling of senescent cell turnover circuits indicated their saturation of removal in aging (*6*). Upregulation of PD-L1 stability in senescent cells can explain the intrinsic mechanism senescent cells employ to inhibit their removal and promote accumulation. Following damage, the buildup of PD-L1-positive senescent cells can be resolved efficiently in young compared to aged organisms as signals driving PD-L1 expression decline with injury resolution. Notably, PD-L1 is also upregulated on many cells regardless of p16 expression. Thus, while antibodies against PD-L1 are a promising strategy to eliminate PD-L1-positive senescent cells, they could also activate an immune response against PD-L1-positive non-senescent cells. Therefore, targeting PD-L1 in combination with other markers and pathways of senescent cells may offer therapeutic opportunities to treat senescence-mediated age-associated diseases.

p16-mediated elevation of PD-L1 in senescent cells could play a functional role in both pathological and physiological conditions. For instance, recently described p16-positive senescent cells in lung regeneration (*34*), could upregulate PD-L1 to evade immune-mediated clearance, which otherwise would be detrimental to tissue integrity. However, persistent senescent cells with elevation of PD-L1 during chronic conditions might be associated with immunosuppression, possibly contributing to compromised immune responses and increased senescent cell burden in aging and chronic inflammation.

The distribution of cells in the human body predicts macrophages to be one of the most abundant resident immune cells in non-lymphatic organs, comprising about 40% of the total immune cell population in the lungs (*35*). Moreover, aging of the immune system is characterized by decreased lymphopoiesis with reduced adaptive immunity, and increased myelopoiesis, which can further contribute to an increase in macrophage population in some organs by several folds (*36, 37*). Interestingly, age-related skewing of the immune system towards myelopoiesis, which underlies inflammaging and myeloid-based pathologies, can be targeted by the depletion of myeloid-biased haematopoietic stem cells to rejuvenate aged immunity (*38*). These findings highlight the central role of myeloid lineage, including macrophages, in the aging of the immune system. Recently immunosenescence of myeloid cells, including senescent AM, was suggested to play an active role in systemic aging and diseases (*13, 39-41*). Senescence of macrophages could contribute to their proinflammatory responses, but also compromised immune functions, leading to an increased senescence burden in tissues. Our data suggest that anti-PD-L1 antibodies could be a promising approach to activate the immune response, deplete senescent macrophages from tissues in aging and chronic inflammation, and ameliorate senescence-associated damage and systemic inflammation.

Blocking PD-1 on T lymphocytes was shown to improve senescence surveillance in the liver (*32*). Interestingly, our data show that only anti-PD-L1 antibodies engaging Fcγ receptors on effector cells, but not blocking anti-PD1 antibodies, led to the depletion of $p16^{+}PD\text{-}L1^{+}$ cells in the inflamed lungs. The PD-1-PD-L1 checkpoint is a complex mechanism at the centre of the regulation of immune responses and, therefore, different antibodies targeting this axis may lead to non-symmetrical responses. The role of PD-L1 is not restricted to immunosuppression via its interaction with PD1 receptors on lymphocytes (*42*). PD-L1 induces intracellular signaling that can enhance the survival of PD-L1-expressing cells, regulate their stress responses, and confer resistance toward pro-apoptotic stimuli (*43*). Our study highlights the complexity of the mechanism regulating immune surveillance of senescent cells and provides the basis for further studies.

In conclusion, we have identified that senescent cells upregulate the stability of PD-L1 in a p16-dependent manner and exploit the PD-L1 signaling to regulate immune responses. Senescent cells use immune checkpoint PD-L1 as an intrinsic mechanism to control their immunosurveillance. These results strongly suggest that persistent senescent cells expressing PD-L1 might lead to dysfunctional immune responses and an unbalanced inflammatory status, eventually resulting in chronic low-grade inflammation. Therefore, targeting PD-L1 on senescent cells not only enhances senescence immunosurveillance but also alleviates senescence-associated inflammaging.

Acknowledgements:

We thank S. Jung for helpful advice and comments on the manuscript, N. Cohen for help with IV injections of anti-PD-L1 antibody, O. Regev and S. Kozlovski for help with bronchoalveolar lavage, M. Tsoory for help with animal experiments, S. Lev for the help with lentivirus production and availability of virus facility, and S. Reich-Zeliger for stimulating discussions. V.K. is an incumbent of The Georg F. Duckwitz Professorial Chair.

Funding:

European Research Council grant 856487 (UA, VK)

Israel Science Foundation grant 2633/17; 1626/20 (VK)

Israel Ministry of Health 3-15100 (VK)

DFG - CRC 1506 “Aging at Interfaces” (VK, WW)

Weizmann – Belle S. and Irving E. Meller Center for the Biology and Aging (VK)

Sagol Institute for Longevity Research (VK)

Minerva Center on “Aging, from physical materials to human tissues” (VK)

Author contributions:

Conceptualization: JM, AA, VK

Methodology: JM, AA, AM, YK, TMS, EH

Investigation: JM, AA, AMay, LR, RC, JK, TL, AMai, IS, JFPC, WW

Visualization: JM, AM, TL

Funding acquisition: VK, UA, IA

Project administration: VK

Supervision: VK, UA, IA

Writing – original draft: JM

Writing – review & editing: JM, VK

Competing interests: JM, AA, AM, UA, and VK are co-inventors on provisional patent application related to the topic of this study. The remaining authors declare no competing interests.

Figure Legends

Fig 1. PD-L1 upregulation correlates with p16 expression in aging

(A) Representative t-SNE plots of immune cell (CD45+) populations identified in 50,000 cells from all lung samples of old and young mice (left). Immune cell type distribution in young and old mice (right). Significantly changed populations are marked with an arrow (right). **(B)** The frequency of indicated immune cell types in young and old mice. **(C)** The heatmap of the change in the enrichment of senescence-related proteins in old mice for indicated immune cell types. **(D)** Mean expression of PD-L1 in the identified immune cell populations. **(E)** Mean expression of PD-L1 in 10% highest and 10% lowest p16-expressing cells within alveolar macrophage population in young and old mice. **(F)** Spearman correlation between p16 and PD-L1 protein expression in alveolar macrophages in young and old mice. AM cells were binned into 12 bins in old mice with a median of 740 cells per bin, and 11 bins in young mice with a median of 350 cells per bin. **(G)** Scatter plot showing fold change in expression of senescence-related markers between p16 high and p16 low expressing cells in alveolar macrophages in young (n=4) and old (n=4) mice. A diagonal line marks an equal fold change between young and old. **(H)** Mean expression of PD-L1 between 10% highest and 10% lowest p16 expressing cells within lung epithelium in young and old mice. **(I)** Spearman correlation between p16 and PD-L1 expression in lung epithelium in young and old mice. Epithelium cells in young and old mice were binned into 18 bins with a median of 14000 cells per bin. **(J)** Scatter plot showing fold change in expression of senescence-related markers between p16 high and p16 low expressing cells in the epithelium in young (n=8) and old (n=8) mice. **(F, I)** Spearman correlation coefficient (r) and associated p-value (p). Single cells were ranked by p16 expression level in bins from low to high. For each bin, the mean expression level of PD-L1 is shown. Alveolar macrophages (AM) and Interstitial Macrophages (IM). (B, D) Two-sided or (E-J) One-sided Whitney-Mann U test was used for statistical analysis. Error bars, mean ± SEM. *$p < 0.05$, **$p < 0.01$, ***$p < 0.001$. (B-G) young (n=4), old (n=4), (H-J) young (n=8), old (n=8). Experiments were repeated three times independently with similar results. Source numerical data are available in source data.

Fig 2. PD-L1 upregulation correlates with p16 expression in chronic inflammation

(A) Principal component analysis of CD45-CD31- cells from control (PBS, Ctrl) and chronically inflamed (LPS, Infl) lungs identifies three clusters (1, 2, and 3) based on their PC values. **(B)** Cell density map for each cluster shown as a difference in Kernel density distribution between Ctrl and Infl condition. Quantification of the fold change of cell frequency for each cluster (right). Error bars were estimated by bootstrapping. 10^4 cells were sampled from each cluster with sampling repeated 10^4 times. **(C)** The expression intensity distribution of epithelial marker (EpCAM) and fibroblast markers (CD90.2, CD140a, and CD140b) for identified clusters. Statistical significance was calculated by the Kruskal-Wallis test. **(D)** Volcano plot displaying enrichment of senescence-related proteins and depletion of the proliferation marker Ki-67 within cluster 1 in comparison to clusters 2 and 3. **(E)** The expression intensity distribution of the indicated proteins between Ctrl and Infl mice within cluster 1. **(F)** Representative t-SNE plots of immune cell (CD45+) populations identified in 50,000 cells from all lung samples of Ctrl and Infl mice (left). Immune cell types distribution in Ctrl and Infl mice. Significantly changed populations of alveolar (AM) and interstitial (IM) macrophages are marked with an arrow (right). **(G)** Frequency of AM and IM in the lungs of Ctrl and Infl mice. **(H)** The change in

the enrichment of senescence-related proteins in Infl mice for indicated immune cell types. **(I)** Mean expression of PD-L1 between identified immune cell populations. **(J)** Mean p16 (left) and PD-L1 (right) expression between AM and IM. **(K)** Alveolar macrophages were binned into 8 bins in Ctrl and 13 bins in Infl with a median of 80 and 1900 cells per bin respectively. Spearman correlation coefficient (r) between p16 and PD-L1 expression in AM of Ctrl and Infl mice and associated p-value (p). Single cells were ranked by p16 expression level in bins from low to high. For each bin, the mean expression level of PD-L1 is shown. **(L)** Mean PD-L1 expression in 10% highest and 10% lowest p16 expressing cells within AM in lungs of Ctrl and Infl mice. (E, K-L) One-sided or (G, I) two-sided Mann-Whitney test was used for statistical analysis unless otherwise noted. Error bars, mean ± SEM. *$p < 0.05$, **$p < 0.01$, ***$p < 0.001$, (A-L) control (n=5-7), Infl (n=5-7). Experiments were repeated three times independently with similar results. Source numerical data are available in source data.

Fig 3. p16 increases the stability of PD-L1 protein in senescent cells.

(A-C) Flow cytometry analysis of PD-L1 expression in DNA damage-induced senescence (D-Sen), Replicative senescence (RIS), and in cells with p16 overexpression (p16 OE) compared to control cells. Primary Mouse Lung Fibroblasts (CCL-206) (A and C), and Primary Human Lung Fibroblasts (IMR-90) were used in these experiments (B). (n=3-8) **(D-E)** PD-L1 protein expression in growing IMR90 cells treated with CDK4/6 inhibitors (D) Palbociclib (Palbo) or (E) Abemaciclib (Abem) or vehicle (control). (n=6-7) **(F)** PD-L1 protein expression in D-Sen treated with siControl or siCDKN2A. (n=9) **(G)** ELISA-based measurement of PD-L1 protein levels in D-Sen treated with siControl or siCDKN2A and cycloheximide (CHX). (n=3) **(H-K)** Immunoblot analysis of whole cell lysates derived from (H) Gr and D-Sen cells, (I) D-Sen cells treated with siControl and siCDKN2A, and (K) Gr and D-Sen cells treated with MG132 or vehicle (negative control) (n=3). (**J)** Immunoblot analysis of Ubiquitin in immunoprecipitated PD-L1 protein derived from Gr and D-Sen cells. **(L)** Quantification of $p16^+$, PD-$L1^+$, and PD-$L1^+p16^+$cells in normal lung tissue (n=3) and human lung pathologies: emphysema (n=3), fibrosis (n=3), adenocarcinoma (n=3), and squamous cell carcinoma (n=3). **(M)** Representative immunofluorescence image of p16 (red) and PD-L1 (green) staining in emphysema patient. Blue, nuclei stain by DAPI. Scale bar indicates 10μm. Image is representative of (n=4) emphysema lung specimens. PD-L1 expression in A-F was quantified by flow cytometry analysis as median fluorescent intensity (MFI). (A, C, G) Two-tailed unpaired Student t-test; (D-F) Two-tailed paired Student t-test, Error bars, mean ± SEM. *$p < 0.05$, **$p < 0.01$, ***$p < 0.001$ (B, L) One-way ANOVA; Error bars, mean ± SEM. **$p < 0.01$, ****$p < 0.0001$. A-K experiments were repeated three times independently with similar results. Source numerical data and unprocessed blots are available in source data.

Fig 4. Anti-PD-L1, but not anti-PD-1, antibody depletes p16, PD-L1-positive cells *in vivo*

(A) Imaging Flow Cytometry analysis of subcellular localization of p16 and PD-L1 staining within the alveolar macrophage (AM) population. Representative images of (a) $CD45^+$PD-$L1^+p16^+$, (b) $CD45^+$PD-$L1^-p16^+$, (c) $CD45^+$PD-$L1^+p16^-$ cells. Bright-field (BF). Scale bars indicate 10μm. Images are representative from three mice repeated independently with similar results. **(B)** INs-Seq of $p16^+$ AM. Gene Set Enrichment Analysis (GSEA) of $p16^+$ and $p16^-$ AM. Control (n=4), Infl (n=4). DESeq2 was used to derive gene fold-changes for p16+ vs. p16- macrophages, controlling for treatment (LPS/PBS) as a covariant. **(C-D)** Flow cytometry analysis of lung. **(C)** Percentage of $Foxp3^+$ Tregs within CD4

population. **(D)** Percentage of CD4 Foxp3$^+$ Tregs expressing PD1. **(E)** Experimental setup: mice exposed daily to either PBS (Ctrl) or LPS (Infl) inhalations for 5 days received anti-PD1, anti-PD-L1, or matched IgG control as indicated, and lungs and bronchoalveolar lavage (BAL) were analysed 48h after the last inhalation. **(F-G)** Flow cytometry analysis of lung **(F)** or BAL **(G)** from mice treated as in E. **(F)** Percentage of p16$^+$PD-L1$^+$ cells within CD45$^+$ or AM. **(G)** Percentage of CD8 T cells positive for ICOS, CD25, CD44 and CD69.
(C-D) Two-sided Mann-Whitney test was used for statistical analysis, error bars, mean ± SEM ***p < 0.001, (F-G) one-way ANOVA; n=3, Error bars, mean ± SEM. *p < 0.05, **p < 0.01, ***p < 0.001; (B-D) control (n=5-9), Infl (n=5-7); (F-G) LPS + IgG (n=11), LPS + anti-PD1 (n=10), LPS + anti-PD-L1 (n=10). C-G experiments were repeated three times independently with similar results. Source numerical data are available in source data.

Fig 5. Anti-PD-L1 antibody depletes p16, PD-L1-positive cells in aging and chronic lung inflammation

(A) Experimental setup: Young or old mice received an anti-PD-L1 or matched IgG control as indicated, and their lungs and blood were analysed 48h after the last injection. **(B-C)** Flow cytometry analysis of lungs from mice treated as in A. **(B)** Percentage of p16$^+$PD-L1$^+$ cells within CD45$^+$ or AM. **(C)** Percentage of CD8 T cells positive for ICOS, CD25, CD44, CD69 and PD1. **(D)** Plasma levels of IFN-γ and IL10. **(E)** Experimental setup: mice were exposed 3 times a week for 10 weeks to LPS (Infl) inhalations and anti-PD-L1 or matched IgG control as indicated, and their lungs were analysed 48h after the last inhalation. Naive mice were the control group (Ctrl). **(F)** Percentage of p16$^+$PD-L1$^+$ cells within CD45$^+$ or AM. **(H)** Senescence-associated gene expression in the lungs of naïve mice compared to the ones with chronic inflammation, treated with anti-PD-L1, or matched IgG control.
For all experiments statistical significance was calculated using one-way ANOVA; Error bars, and mean ± SEM. *p < 0.05, **p < 0.01, ***p < 0.001, ****p < 0.0001; (A-D) young (n=7), old + IgG (n=7), old + anti-PD-L1 (n=8); (E-H) naive (n=6-7), Infl + IgG (n=7-10), Infl + anti-PD-L1 (n=7-8). Experiments were repeated three times independently with similar results. Source numerical data are available in source data.

References

1. B. G. Childs, M. Durik, D. J. Baker, J. M. van Deursen, Cellular senescence in aging and age-related disease: from mechanisms to therapy. *Nat Med* **21**, 1424-1435 (2015).
2. D. J. Baker *et al.*, Naturally occurring p16(Ink4a)-positive cells shorten healthy lifespan. *Nature* **530**, 184-189 (2016).
3. D. J. Baker *et al.*, Clearance of p16Ink4a-positive senescent cells delays ageing-associated disorders. *Nature* **479**, 232-236 (2011).
4. S. M. Schoenwaelder *et al.*, Bcl-xL-inhibitory BH3 mimetics can induce a transient thrombocytopathy that undermines the hemostatic function of platelets. *Blood* **118**, 1663-1674 (2011).
5. B. I. Pereira *et al.*, Senescent cells evade immune clearance via HLA-E-mediated NK and CD8(+) T cell inhibition. *Nature communications* **10**, 2387 (2019).
6. O. Karin, A. Agrawal, Z. Porat, V. Krizhanovsky, U. Alon, Senescent cell turnover slows with age providing an explanation for the Gompertz law. *Nature communications* **10**, 5495 (2019).
7. M. J. Yousefzadeh *et al.*, An aged immune system drives senescence and ageing of solid organs. *Nature* **594**, 100-105 (2021).
8. Y. Ovadya *et al.*, Impaired immune surveillance accelerates accumulation of senescent cells and aging. *Nature communications* **9**, 5435 (2018).
9. R. Yosef *et al.*, p21 maintains senescent cell viability under persistent DNA damage response by restraining JNK and caspase signaling. *EMBO J*, (2017).
10. R. Yosef *et al.*, Directed elimination of senescent cells by inhibition of BCL-W and BCL-XL. *Nature communications* **7**, 11190 (2016).
11. J. Majewska, V. Krizhanovsky, Breathe it in - Spotlight on senescence and regeneration in the lung. *Mech Ageing Dev* **199**, 111550 (2021).
12. A. Biran *et al.*, Quantitative identification of senescent cells in aging and disease. *Aging Cell* **16**, 661-671 (2017).
13. L. I. Prieto *et al.*, Senescent alveolar macrophages promote early-stage lung tumorigenesis. *Cancer Cell* **41**, 1261-1275.e1266 (2023).
14. A. Sagiv *et al.*, p53 in Bronchial Club Cells Facilitates Chronic Lung Inflammation by Promoting Senescence. *Cell reports* **22**, 3468-3479 (2018).
15. P. J. Barnes *et al.*, Chronic obstructive pulmonary disease. *Nat Rev Dis Primers* **1**, 15076 (2015).
16. R. J. Hewitt, C. M. Lloyd, Regulation of immune responses by the airway epithelial cell landscape. *Nature Reviews Immunology* **21**, 347-362 (2021).
17. F. M. Carlier, C. de Fays, C. Pilette, Epithelial Barrier Dysfunction in Chronic Respiratory Diseases. *Frontiers in physiology* **12**, (2021).
18. F. Rodier *et al.*, DNA-SCARS: distinct nuclear structures that sustain damage-induced senescence growth arrest and inflammatory cytokine secretion. *J Cell Sci* **124**, 68-81 (2011).
19. U. Asghar, A. K. Witkiewicz, N. C. Turner, E. S. Knudsen, The history and future of targeting cyclin-dependent kinases in cancer therapy. *Nat Rev Drug Discov* **14**, 130-146 (2015).
20. K. Flick, P. Kaiser, Protein degradation and the stress response. *Semin Cell Dev Biol* **23**, 515-522 (2012).
21. Q. Gou *et al.*, PD-L1 degradation pathway and immunotherapy for cancer. *Cell death & disease* **11**, 955 (2020).
22. X. L. Ang, J. Wade Harper, SCF-mediated protein degradation and cell cycle control. *Oncogene* **24**, 2860-2870 (2005).
23. J. H. Cha, L. C. Chan, C. W. Li, J. L. Hsu, M. C. Hung, Mechanisms Controlling PD-L1 Expression in Cancer. *Mol Cell* **76**, 359-370 (2019).
24. A. Onorati *et al.*, Upregulation of PD-L1 in Senescence and Aging. *Mol Cell Biol* **42**, e0017122 (2022).

25. J. Zhang *et al.*, Cyclin D–CDK4 kinase destabilizes PD-L1 via cullin 3–SPOP to control cancer immune surveillance. *Nature* **553**, 91-95 (2018).
26. F. Sato *et al.*, Prognostic impact of p16 and PD-L1 expression in patients with oropharyngeal squamous cell carcinoma receiving a definitive treatment. *J Clin Pathol* **72**, 542-549 (2019).
27. Y. Katzenelenbogen *et al.*, Coupled scRNA-Seq and Intracellular Protein Activity Reveal an Immunosuppressive Role of TREM2 in Cancer. *Cell* **182**, 872-885.e819 (2020).
28. M. M. Coleman *et al.*, Alveolar macrophages contribute to respiratory tolerance by inducing FoxP3 expression in naive T cells. *Am J Respir Cell Mol Biol* **48**, 773-780 (2013).
29. D. M. Pardoll, The blockade of immune checkpoints in cancer immunotherapy. *Nature Reviews Cancer* **12**, 252-264 (2012).
30. R. Dahan *et al.*, FcγRs Modulate the Anti-tumor Activity of Antibodies Targeting the PD-1/PD-L1 Axis. *Cancer Cell* **28**, 285-295 (2015).
31. P. Bhat, G. Leggatt, N. Waterhouse, I. H. Frazer, Interferon-γ derived from cytotoxic lymphocytes directly enhances their motility and cytotoxicity. *Cell death & disease* **8**, e2836 (2017).
32. T.-W. Wang *et al.*, Blocking PD-L1–PD-1 improves senescence surveillance and ageing phenotypes. *Nature* **611**, 358-364 (2022).
33. A. Alpert *et al.*, A clinically meaningful metric of immune age derived from high-dimensional longitudinal monitoring. *Nat Med* **25**, 487-495 (2019).
34. N. S. Reyes *et al.*, Sentinel p16(INK4a+) cells in the basement membrane form a reparative niche in the lung. *Science* **378**, 192-201 (2022).
35. R. Sender *et al.*, The total mass, number, and distribution of immune cells in the human body. *Proceedings of the National Academy of Sciences* **120**, e2308511120 (2023).
36. C. N. Lumeng *et al.*, Aging Is Associated with an Increase in T Cells and Inflammatory Macrophages in Visceral Adipose Tissue. *The Journal of Immunology* **187**, 6208-6216 (2011).
37. S. N. Hilmer, V. C. Cogger, D. G. Le Couteur, Basal activity of Kupffer cells increases with old age. *J Gerontol A Biol Sci Med Sci* **62**, 973-978 (2007).
38. J. B. Ross *et al.*, Depleting myeloid-biased haematopoietic stem cells rejuvenates aged immunity. *Nature* **628**, 162-170 (2024).
39. Z. Zhou *et al.*, Type 2 cytokine signaling in macrophages protects from cellular senescence and organismal aging. *Immunity*, (2024).
40. C. M. Wilk *et al.*, Circulating senescent myeloid cells infiltrate the brain and cause neurodegeneration in histiocytic disorders. *Immunity* **56**, 2790-2802.e2796 (2023).
41. S. Haston *et al.*, Clearance of senescent macrophages ameliorates tumorigenesis in KRAS-driven lung cancer. *Cancer Cell* **41**, 1242-1260.e1246 (2023).
42. J. Chen, C. C. Jiang, L. Jin, X. D. Zhang, Regulation of PD-L1: a novel role of pro-survival signalling in cancer. *Annals of Oncology* **27**, 409-416 (2016).
43. D. Escors *et al.*, The intracellular signalosome of PD-L1 in cancer cells. *Signal Transduction and Targeted Therapy* **3**, 26 (2018).

Methods

Cell Culture. Mouse lung fibroblasts CCL-206, human lung fibroblasts IMR-90, and HEK293T were purchased from ATCC (#CCL-206, #CCL-186, and #CRL-3216 respectively). Cells were cultured to 70% confluency in Dulbecco's modified Eagle (DMEM) medium supplemented with 10% fetal bovine serum (FBS) and 1% penicillin–streptomycin. To induce senescence, cells were treated with 50 □M etoposide (Sigma, #E1383) for 48h, washed 3 times with PBS, and cultured for additional 5-7 days in DMEM medium. Replicative senescence (RIS) was induced by long-term passaging of the cells in tissue culture. Cells developed senescence phenotype after 35 population doublings. On the day of the experiment, cells were detached using trypsin.

Lentivirus production and infection. Generation of lentiviruses and their infection of cells was performed as described previously (*44*). Lentiviruses were generated by co-transfecting HEK293T cells with 4 μg of pLX401-INK4A (AddGene, #121919), and 2 μg each of pLP/VSVG, pLP1, pLP2 plasmids using Lipofectamine2000 (Invitrogen, #11668019). Growth media was exchanged the following day, and lentivirus-containing supernatant was harvested 48h later. CCL-206, IMR-90, and HEK293T cells were infected with the indicated viruses for 12h, washed 3 times with PBS, and cultured for an additional 24h in RPMI medium. For selection cells were re-seeded in fresh RPMI medium with 1 $\mu g\ ml^{-1}$ of puromycin (Gibco, #A1113803) for 4-5 days. Doxycycline (Sigma-Aldrich, #D3072) was added to the medium at a concentration of 5 or 10 $\mu g\ ml^{-1}$ for inducible expression of the plasmid system.

siRNA. Cells were transfected overnight with 50nM of ON-TARGETplus SMARTpool siRNA targeting CDKN2A (#L-011007-00-0005) or with non-targeting siRNA pool (#D-001810-10-20) as control (Dharmacon). 24h post transfection remaining adherent cells were harvested.

CDK4/6 inhibitors. Abemaciclib (Pubchem, #LY2835219) and palbociclib (Sigma, #PZ0383) were dissolved in DMSO (vehicle) to yield 10 mM stock solutions and stored at 80□C. IMR90 cells were treated with DMEM medium supplemented with either 1uM abemaciclib, palbociclib or equivalent amount of DMSO for 48h.

Proteasome inhibition. IMR90 cells were treated with DMEM medium supplemented with either 10 μM MG132 (Sigma, #M7449) or equivalent amount of DMSO for 3h.

Immunoblot and immunoprecipitation assay. Cells were incubated in RIPA lysis buffer containing protease inhibitor cocktail (1:100) (Sigma, #P8340) and phosphatase inhibitor cocktail (1:100) (Sigma, #p5726) for 20 min on ice. Lysates were spun down for 15 min at 13,000 rpm and 4°C, and protein

concentrations were determined with BCA assay (Thermo Scientific). Equal amounts of protein were resolved by SDS–PAGE and immunoblotted using β-TrCP (Cell Signalling Technology, CST-4394S), p16 (Abcam # Ab108349, human; Abcam #Ab211542, mouse), vinculin (Abcam #Ab129002), PD-L1 (Cell Signalling Technology, #CST-13684, human, Abcam #Ab213480, mouse), appropriate HRP-conjugated secondary antibody and ECL visualization.

For immunoprecipitations analysis, cells were lysed in HNTG buffer (0.05M Hepes pH 7.5, 10% Glycerol, 0.15M NaCl, 1% Triton X-100, 0.001M EDTA, 0.001M EGTA, 0.01M NaF, 0.025M □-glycerol phosphate) supplemented with protease inhibitor cocktail (1:100) (Sigma, #P8340) and phosphatase inhibitor cocktail (1:100) (Sigma, #P5726). 2,000 μg of total cell lysates were incubated with previously coated protein A/G agarose beads (Santa Cruz Biotechnology, #2003) with anti-PD-L1 antibody (3ug/ml) (Cell Signalling Technology, #13684) overnight at 4°C with gentle rotation. The beads were thoroughly washed with HNTG buffer and eluted with 6×SDS loading buffer by boiling at 95°C for 10 min. Ubiquitination of PD-L1 was measured by immunoblotting with anti-Ubiquitin antibody (Santa Cruz Biotechnology, #8017).

Cycloheximide Chase Assay. 24h following transfection with siRNA, senescent IMR90 cells were treated with 200 μM cycloheximide (Sigma, #C4859) for 3h. Cells were lysed by incubation with 100 μl of RIPA buffer (supplemented with PMSF and protease inhibitor cocktail) for 20 min on ice and protein concentrations were determined using BCA assay. 10 μg of protein lysate was used to measure levels of PD-L1 by the enzyme-linked immunosorbent assay (ELISA), using the PD-L1/B7-H1 Quantikine ELISA Immunoassay kit (R&D, #DB7H10), according to the manufacturer's protocol. The optical density of each well was measured with the Infinite 200 plate reader (Tecan) at 450 nm with wavelength correction set at 540 nm. The experiment was performed twice and each sample was performed in duplicate.

Immunofluorescent staining of human tissue microarray. FFPE sections of human lung tissue microarray (US Biomax, #LC487) were incubated at 60°C for 60 min, deparaffinized, and incubated in acetone for 7 min at -20°C, followed by subsequent incubation with 3% H_2O_2 for 15 min at room temperature to block endogenous peroxidase activity. Antigen retrieval was performed in a microwave (3 min at full power, 1000 W, then 20 min at 20% of full power) in Tris-EDTA buffer (pH 9.0). Slide was blocked with 20% NHS + 0.5% Triton in PBS and primary antibodies were diluted in 2% NHS + 0.5% Triton in PBS (PBST) (p16 1:30, Abcam #Ab108349; PD-L1 1:100, Abcam #Ab213524) in a multiplexed manner with the OPAL reagents (Akoya Bioscience), each one O.N. at 4°C. Following over-night incubation with the first primary antibody, the slide was washed with PBS, incubated in 2% NHS in PBS with secondary antibody conjugated to HRP (1:100) for 90 min, washed again, and incubated with OPAL reagents for 15 min. The slide was then washed and microwaved (as described

above), washed, stained with the next primary antibody and with DAPI at the end of the cycle, and mounted. We used the following staining sequence: p16 → PD-L1→ DAPI. Each antibody was validated separately, and then multiplexed immunofluorescence (MxIF) was optimized to confirm that the antibody signal was not lost or changed due to the multistep protocol. Slides were imaged with an Eclipse Ni-U microscope (Nikon), connected to a color camera (DS-Ri1, Nikon, x20), and DAPI, Cy3 and Cy5 cubes. Images were analyzed using the Fiji v2.6.0 software. The QuePath v0.4.4 software was used for the identification and quantification of cells positive for the fluorescent signal of each marker.

Mice. Female C57BL/6 mice 10 - 14 weeks of age (young) or 24 months old (old) were used in all experiments. Mice were purchased from Harlan Laboratories. All mice were housed and maintained under specific pathogen-free conditions at the Weizmann Institute of Science in accordance with national animal care guidelines. The housing conditions were: 12-hour dark/light cycle (lights on at 8 am), 22°C temperature, and 30-70% humidity. All procedures were performed in accordance with the protocols approved by the Weizmann Institute Animal Care and Use Committee (03320423-1, 06900820-2, 02720418-2, 05410621-3, 04000523-1, 04040523-2).

LPS exposure and Treatment. For chronic LPS exposure, mice were exposed to an aerosolized PBS alone or PBS containing Escherichia coli LPS (0.5 mg/ml; Sigma, #L2630) for 30 min, 3 times a week for 10 weeks, in a custom-built cylindrical chamber as described previously (*14*). For short-term 5-day LPS exposure, mice were exposed as in chronic exposure, but only for 5 constitutive days. Mice were sacrificed and lungs were harvested 48h after the last exposure.

For the ICB treatment mice received intravenous injection of 200 μg anti-PD-L1 (Ichorbio, #ICH1086), 200 μg anti-PD1 (Ichorbio, #ICH1091), or 200 μg isotype control IgG2b (Ichorbio, #ICH2243).

In short-term 5-day LPS exposure, mice were treated with ICB on the second and fifth day of LPS inhalation. Old mice and mice undergoing chronic LPS exposure were treated with ICB in 5 doses within 3 weeks, and the mice were euthanized two days after the final injection.

BAL fluid was collected from perfused lungs by double washing with 1 mL PBS through a tracheal catheter as previously described (*14*).

Measurement of cytokines levels in plasma. Blood was taken from the mice through cardiac puncture. To obtain plasma, blood samples were diluted 1:1 with PBS containing 1mM EDTA upon the collection and then centrifuged at 3,400*g* for 15 min at 4 °C. Plasma levels of cytokines were measured by Milliplex MAP Mouse High Sensitivity T Cell Panel (cat no. MHSTCMAG-70K; Millipore) on Luminex (MAGPIX) following the manufacturer's instructions. All samples were assayed in duplicate and mean values analysed. BELYSA v1.2 software (Millipore) was applied for data analysis. Concentrations are reported in pg/mL.

Epigenetic age predictions. Genomic DNA was isolated from whole blood using a Qiagen QIAamp DNA Mini and Blood Mini Kit (Qiagen, Hilden, Germany) and DNA concentrations were measured with a NanoDrop2000 spectrophotometer (Thermo Scientific, Wilmington, United States). 500ng of genomic DNA was bisulfite converted with the Zymo Research Group EZ DNA Methylation Kit (Zymo Research, Irvine, United States). Pyrosequencing was performed with the PyroMark Q48 Autoprep system (Qiagen, Hilden, Germany), and DNA methylation percentages were obtained for age-related CpGs in *Aspa*, *Wnt3a*, *Prima1*, and *Hsf4* for the samples from young, and old mice treated with anti-PD-L1 or matched isotype control. Primers, PCR conditions, and targeted epigenetic age calculations were used, as described before (*45*).

Tissue Dissociation. To achieve single-cell suspension from the lung, mice were euthanized by administration of xylazine/ketamine and then perfused by injecting cold PBS via the right ventricle before lung dissection. Lung tissues were dissected from mice, cut into small fragments, and suspended in 1.5 ml of Dulbecco's modified Eagle medium/F12 medium (Invitrogen, #11330-032) containing elastase (3 U/ml, Worthington, #LS002279), collagenase type IV (1 mg/ml, Thermo Scientific, #17104019) and DNase I (0.5 mg/ml, Roche, #10104159001) and incubated at 37 °C for 20 min with frequent agitation. After dissociation procedure, cells were washed with an equal volume of DMEM/F12 supplemented with 10% FBS and 1% penicillin–streptomycin (Thermo Scientific), filtered through a 100-µm cell strainer, and centrifuged at 380*g* for 5 min at 4 °C. Pelleted cells were resuspended in red blood cell ACK lysis buffer (Gibco, #A1049201), incubated for 2 min at 25°C, centrifuged at 380g for 5 min at 4°C and then resuspended in ice-cold FACS buffer (PBS supplemented with 2mM ethylenediaminetetraacetic acid, pH 8 and 0.5% BSA).

Flow cytometry. IMR-90 cells were stained with Zombie Aqua Viability fixable stain (#423101) or Sytox Blue (Invitrogen, #34857) for evaluation of live/dead cells, followed by antibody Brilliant Violet 711-PD-L1 (#329721) or isotype control (#400353) staining (all from Biolegend).

Lung single cell suspension was stained with anti-mouse CD16/32 (eBioscience, #14-0161-82) to block Fc receptors before labeling with fluorescent antibodies against cell-surface epitopes. For samples which were used for p16 intracellular staining, we used following antibodies for extracellular staining: Brilliant Violet 605-CD45 (#103140), FITC-CD11c (#117306), Brilliant Violet 421-SiglecF (#155509) purchased from Biolegend. We used two clones of PD-L1 antibody (either Brilliant Violet 785-PD-L1, #124331 or PE-Cy5-PD-L1, #124344 both clone 10F.9G2, and PE-PD-L1, #153611, clone MIH6) purchased from Biolegend, which yielded similar results. Then cells were fixed with 90% methanol for 10 min at 4°C. All centrifugation steps after fixation were done at 850*g* for 5 min at 4 °C. For intracellular staining, cells were stained with p16 antibody (Abcam, #Ab54210) conjugated to Alexa

Fluor 647 fluorophore (Thermo Scientific, #A20186). Cells were stained with Zombie Aqua Viability fixable stain for evaluation of live/dead cells. For characterization of immune subsets in BAL we used following antibodies: Pacific Blue-CD69 (#104523), Brilliant Violet 605-ICOS (#313537), Brilliant Violet 785-NK1.1 (#108749), PerCP-CD19 (#115531), FITC-CD3 (#100204), PE-CD25 (#102007), PE-Dazzle 595-TIGIT (#142109), PE-Cy5-CD8 (#100709), PE-Cy7-CTLA4 (#106313), APC-LAG3 (#125209), Spark Nir 685-CD4 (#100475), Alexa Fluor700-CD44 (#103025), APC/Cy7-PD1 (#135223), APC Fire810-CD45 (#103173). All antibodies were purchased from Biolegend and diluted 1:100 in FACS buffer before staining. Cell populations were recorded using LSR-II new (BD Biosciences) or Aurora (Cytec), and analyzed using FlowJo v10 software (BD Biosciences) and Prism v7 software.

For imaging flow-cytometry cells were stained with FITC-CD45 (Biolegend, #103107), Brilliant Violet 786-PD-L1 (Biolegend, #124331) and Ax647-p16 (Abcam, #Ab54210, conjugated to Alexa Fluor 647 fluorophore from Thermo Scientific, #A20186). Before acquisition, cells were stained with DAPI and filtered through a 100 µm membrane. All antibodies were diluted 1:100 in FACS buffer before staining. Cells were acquired using ImageStreamX mark II (Amnis, Part of EMD Milipore Merck) and image data analysis was performed using IDEAS v6.2 software as described in previously (*6*).

Mass Cytometry. All antibodies used in the study, their corresponding clone, provider and catalog number are listed in Table 1. Antibodies were obtained in protein-free buffer. Custom metal-conjugated antibodies were generated using MaxPAR antibody labelling kits (Fluidigm) or the MIBItag Conjugation Kit (IONpath) according to the manufacturer's instructions. After metal conjugation, the concentration of each antibody was determined with a Nanodrop (Thermo Scientific), and adjusted to 0.5 mg/ml with Antibody Stabilizer PBS (CANDOR Bioscience, #131050) for long-term storage at 4°C. Lung single-cell suspension was washed once in 1 ml of Cell Staining Buffer (CSB) (Fluidigm, #201068). To ensure homogeneous staining, 4 x 10^6 cells from each sample were used. For viability staining, cells were incubated with 1.25 µM Cell-ID Cisplatin (Fluidigm, #201064) for 3 min before quenching with CSB. Prior to antibody staining, cells were incubated for 10 min at 4°C with anti-mouse CD16/32 (Invitrogen, #14-0161-82) to bloc Fc receptors. Cells were stained with the epithelial or immune-centric antibodies for 45 min at 4°C. An antibody cocktail of extracellular markers was prepared as a master mix and 50 µl of the cocktail was added to the samples resuspended in 50 µl of CSB. Cells were washed twice with CSB, and permeabilized with fixation/permeabilization buffer (eBioscience, #88-8824-00). Then, samples were washed twice with CSB, incubated with 5% goat serum (Sigma, #G-9023) and resuspended in 50 µl of CSB before the addition of 50 µl of cocktail of intracellular antibodies. For DNA-based detection, cells were stained with 125 nM Cell-ID Intercalator-Ir (Fluidigm, #201192A) in PBS with 1.6% PFA (Electron Microscopy Sciences, #15700) overnight at 4°C. Cells were then washed once in CSB, and twice in Maxpar Water (Fluidigm, #201069). For mass

cytometry acquisition, samples were diluted to 3 x 10^5 cells/ml in Maxpar Water containing 1:10 EQ Four Element Calibration Beads (Fluidigm, #201078) and filtered through a 35-µm filtermesh tube (Falcon). For acquisition CyTOF Helios system (Fluidigm) was used and samples were acquired at the rate of 200 events/sec. Data was collected as .fcs files. Data was normalized, and concatented when necessary, via the CyTOF software v7.0 (Fluidigm). Then, the Cytobank platform (Beckman Coulter) was used to gate out the normalization beads according to the 140Ce channel. Next, several gates were applied to gate out live cells for further analysis. First, live single cells were gated using the cisplatin 195Pt, iridium DNA label in 193Ir, followed by the event length, and the Gaussian parameters of width, center, offset and residual channels. To normalize data a hyperbolic arcsine transformation (with a scale factor of 5) was first applied. FlowSOM k-NN clustering and two-dimensions viSNE projections were calculated using Cytobank v9.0 software. Subsequently mass cytometry data was analysed in Matematica (v14.0) and all custom-generated code is available in the AlonLabWIS git.

Flow cytometry cell sorting. Cell populations were sorted using BD FACSAria Fusion flow cytometer (BD Biosciences). Before sorting, all samples were filtered through a 70-mm nylon mesh. Populations that were sorted were epithelial cells (EpCam+ CD31- CD45- Ter119-), alveolar macrophages (CD45+CD11c+SiglecF+ p16 high/low), and CD8a T cells (CD45+SiglecF-CD3+CD8a+). Sytox Blue (Invitrogen, #34857) or Aqua Zombie was used for viability staining. 5,000-1000 live cells were sorted into a low-bind eppendorf tube containing 50 ul of lysis/binding buffer (Invitrogen). Immediately after sorting, samples were spun down, snap frozen and stored at –80°C until further processing.
To sort out lung epithelium, cells were stained with following antibodies: Brilliant Violet BV605-CD31 (#102427), PE-CD45 (#103106), Alexa Fluor 488-EpCam (#118210) all purchased from BioLegend and eFluor450-TER-119 (eBioscience, #48-5921-82). To sort out alveolar macrophages, cells were stained with Brilliant Violet 605-CD45 (#103140), FITC-CD11c (#117306), Brilliant Violet 421-SiglecF (#155509), Brilliant Violet 786-PD-L1 (#124331) all from Biolegend and p16 (Abcam, #Ab54210) conjugated to Alexa Fluor 647 fluorophore (Thermo Scientific, #A20186).
To sort out CD8a T cells, cells were stained with Brilliant Violet 605-CD45 (#103140), Brilliant Violet 421-SiglecF (#155509), FITC-CD3 (#100204), APC-CD8a (#100711). All antibodies were purchased from Biolegend and diluted 1:100 in FACS buffer before staining.

Preparation of libraries for RNA-seq. 10^4 cells of lung epithelium (EpCam+ CD31- CD45-) were sorted into 50 µL of lysis/binding buffer (Life Technologies). mRNA was captured with 15 µl of Dynabeads oligo(dT) (Life Technologies), washed, and eluted at 70°C with 6.1 µl of 10 mM Tris-Cl (pH 7.5). cDNA libraries were prepared from pooled samples of the same cell type (10000 cells per sample) according to a bulk variation of MARSseq (*46*), and were sequenced on Illumina NextSeq500

(Illumina). INs-seq libraries were prepared as previously described (*27*) followed by bulk MARS-sequencing.

RNA-seq analysis. Raw data was processed with the User-friendly Transcriptome Analysis Pipeline (UTAP) (*47*). Only reads with unique mapping to the 3' of RefSeq annotated genes (mm10, NCBI Mus musculus Annotation Release 109) were analyzed. For differential gene expression analysis, we used DESeq2 (*48*), following standard workflow, to analyze RNA-seq count data derived from lung epithelial cells, comparing LPS to PBS. Genes with < 30 UMIs across samples were pre-filtered. Differentially expressed genes (DEGs) were selected to have $fold-change \vee 1.25$ and Benjamini-Hochberg adjusted $P < 0.05$. For Gene set enrichment analysis, we used DESeq2 (*38*) to derive gene fold-changes for LPS vs. PBS epithelial cells, and for p16+ vs. p16- macrophages, controlling for treatment (LPS/PBS) as a covariant. We then applied gene set enrichment analysis (GSEA) to the ranked fold-changes. We used Fast Gene Set Enrichment Analysis ("fgsea") library (*49*) implemented in R to test for enrichment of gene sets (#genes > 10) from the mouse C5 v5p2 gene ontology (GO) collection of the Molecular Signature Database (*50*).

Real-time RT–PCR analysis. mRNA was extracted from 5000 CD8a T cells sorted into 50ul of lysis/binding buffer (Invitrogen) and captured using Dynabeads oligo(dT) (Invitrogen) kit according to the manufacturer's protocols. For lung tissue total RNA was extracted using Qiagen kit. For qPCR analysis, mRNA was reverse transcribed using SuperScript II (Invitrogen, Cat#11904018) and cDNA was diluted 1:10 for qPCR analysis performed using the SYBR Green system. The relative gene expression was determined using the ΔΔCt method and normalization to *Actb*. We used four biological replicates for each condition. One-tailed t-tests were used to perform statistical analysis.
The following primers were used: mouse *Actb*: forward, 5′-GGAGGGGGTTGAGGTGTT-3′, reverse, 5′- TGTGCACTTTTATTGGTCTCAAG-3′; *Ifng*: forward, 5′- TGAACGCTACACACTGCATCTTGG-3′, reverse, 5′-CGACTCCTTTTCCGCTTCCTGAG-3′; *p16*: forward, 5′-TTGGGCGGGCACTGAATCTC-3′, reverse, 5′-AGTCTGTCTGCAGCGGACTC-3′; *p19*: forward, 5′-GCCGCACCGGAATCCT-3′; reverse, 5′- TTGAGCAGAAGAGCTGCTACGT-3′; *p21*: forward, 5′-GACAAGAGGCCCAGTACTTC-3′; reverse, 5′-GCTTGGAGTGATAGAAATCTGTC-3′; *Il-1b:* forward, 5′-GGAGAACCAAGCAACGACAAAATA-3′;reverse, 5′-TGGGGAACTCTGCAGACTCAAAC-3′; *Tnf:* forward, 5′-CCACGCTCTTCTGTCTACTG-3′; reverse, 5′-GATGAGAGGGAGGCCATTTG-3′; *Il-6:* forward, 5′-TAGTCCTTCCTACCCCAATTTCC-3′; reverse, 5′-TTGGTCCTTAGCCACTCCTTC-3′; *CXCL10:* forward, 5′-CCATCAGCACCATGAACC-3′; reverse, 5′-TCCGGATTCAGACATCTC-3′; *HPRT*: forward, 5'-TGACACTGGCAAAACAATGCA-3'; reverse, 5'-GGTCCTTTTCACCAGCAAGCT-3'

Statistics and Reproducibility. For mice experiments, no statistical method was used to predetermine sample sizes. In each experiment number of animals was chosen to have sufficient statistical power based on the literature and experience (*6,7,15*). For cell culture experiments, the sample size was determined to be at least n=3 independent biological repeats, while in each experiment every sample had 3 technical repeats. Data are presented as means ±SEM, unless otherwise noted. Comparisons between two groups were performed by an unpaired two-tailed Student's t-test, unless otherwise noted. Comparisons between the three groups were performed by one-way ANOVA. Chi-squared test was performed for RNA-seq analysis of DEGs. For consistency in comparisons, significance in all figures is denoted as follows: $*P < 0.05$, $**P < 0.01$, $***P < 0.001$, $****P < 0.0001$.

Data availability

All NGS sequencing data in this manuscript are available at NCBI GEO under the accession numbers GSE225285 (INseq data for alveolar macrophages), and GSE225286 (for lung epithelium). Mass cytometry data is available at juliamajewski GitHub (http://github.com/juliamajewski/p16-dependent-increase-of-PD-L1-stability-regulates-immunosurveillance-of-senescent-cells). All other data supporting the findings from this study are available from the corresponding author on reasonable request.

Code availability

Custom-generated code for analysis of mass cytometry data is available in the AlonLabWIS git (https://github.com/AlonLabWIS/Immune-checkpoint-keeps-senescent-cells-alive.git). Custom-generated code for analysis of RNA-Seq data is available at tomerlan git (https://github.com/tomerlan/p16_PDL1).

Methods-only references

44. D. Wiederschain *et al.*, Single-vector inducible lentiviral RNAi system for oncology target validation. *Cell Cycle* **8**, 498-504 (2009).
45. J. F. Perez-Correa, V. Tharmapalan, H. Geiger, W. Wagner, Epigenetic Clocks for Mice Based on Age-Associated Regions That are Conserved Between Mouse Strains and Human. *Front Cell Dev Biol* **10**, 902857 (2022).
46. D. A. Jaitin *et al.*, Massively parallel single-cell RNA-seq for marker-free decomposition of tissues into cell types. *Science* **343**, 776-779 (2014).
47. R. Kohen *et al.*, UTAP: User-friendly Transcriptome Analysis Pipeline. *BMC Bioinformatics* **20**, 154 (2019).
48. M. I. Love, W. Huber, S. Anders, Moderated estimation of fold change and dispersion for RNA-seq data with DESeq2. *Genome Biol* **15**, 550 (2014).

49. G. Korotkevich, V. Sukhov, A. Sergushichev, Fast gene set enrichment analysis. *bioRxiv*, 060012 (2019).
50. A. Liberzon *et al.*, Molecular signatures database (MSigDB) 3.0. *Bioinformatics* **27**, 1739-1740 (2011).

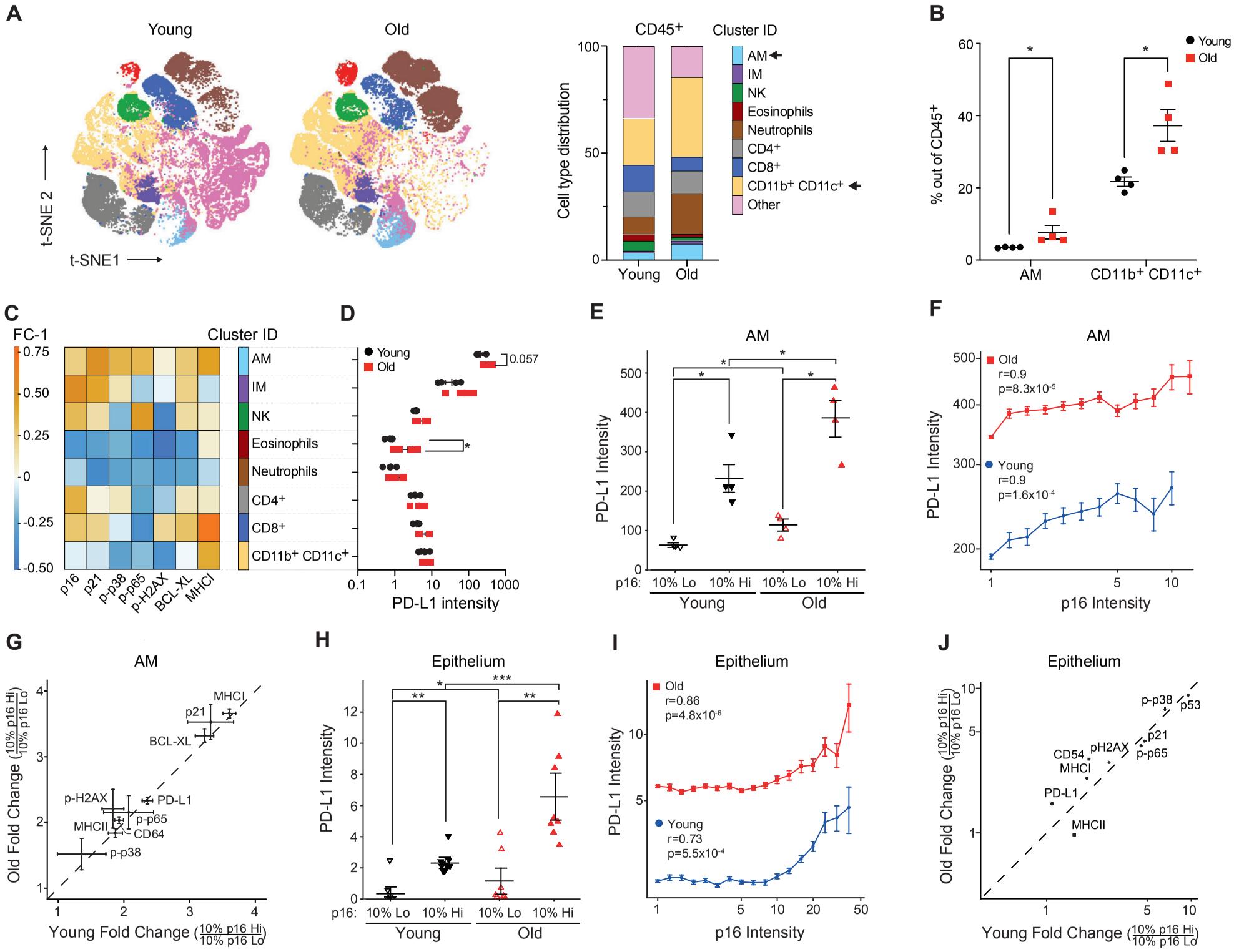
A
Young
Old
t-SNE 2
t-SNE1
CD45+
Cluster ID
AM
IM
NK
Eosinophils
Neutrophils
CD4+
CD8+
CD11b+ CD11c+
Other
Cell type distribution
100
50
0
Young
Old
B
Young
Old
% out of CD45+
60
40
20
0
*
*
AM
CD11b+ CD11c+
C
FC-1
0.75
0.50
0.25
0
-0.25
-0.50
Cluster ID
AM
IM
NK
Eosinophils
Neutrophils
CD4+
CD8+
CD11b+ CD11c+
p16
p21
p-p38
p-p65
p-H2AX
BCL-XL
MHCI
D
Young
Old
0.057
*
0.1
1
10
100
1000
PD-L1 intensity
E
AM
PD-L1 Intensity
500
400
300
200
100
0
*
*
*
*
p16:
10% Lo
10% Hi
10% Lo
10% Hi
Young
Old
F
AM
PD-L1 Intensity
500
400
300
200
Old
r=0.9
p=8.3x10-5
Young
r=0.9
p=1.6x10-4
1
5
10
p16 Intensity
G
AM
Old Fold Change (10% p16 Hi / 10% p16 Lo)
4
3
2
1
MHCI
p21
BCL-XL
p-H2AX
PD-L1
MHCII
p-p65
CD64
p-p38
1
2
3
4
Young Fold Change (10% p16 Hi / 10% p16 Lo)
H
Epithelium
PD-L1 Intensity
12
10
8
6
4
2
0
*
***
**
**
p16:
10% Lo
10% Hi
10% Lo
10% Hi
Young
Old
I
Epithelium
PD-L1 Intensity
10
5
Old
r=0.86
p=4.8x10-6
Young
r=0.73
p=5.5x10-4
1
5
10
20
50
p16 Intensity
J
Epithelium
Old Fold Change (10% p16 Hi / 10% p16 Lo)
10
5
1
p-p38
p53
p21
p-p65
CD54
pH2AX
MHCI
PD-L1
MHCII
1
5
10
Young Fold Change (10% p16 Hi / 10% p16 Lo)

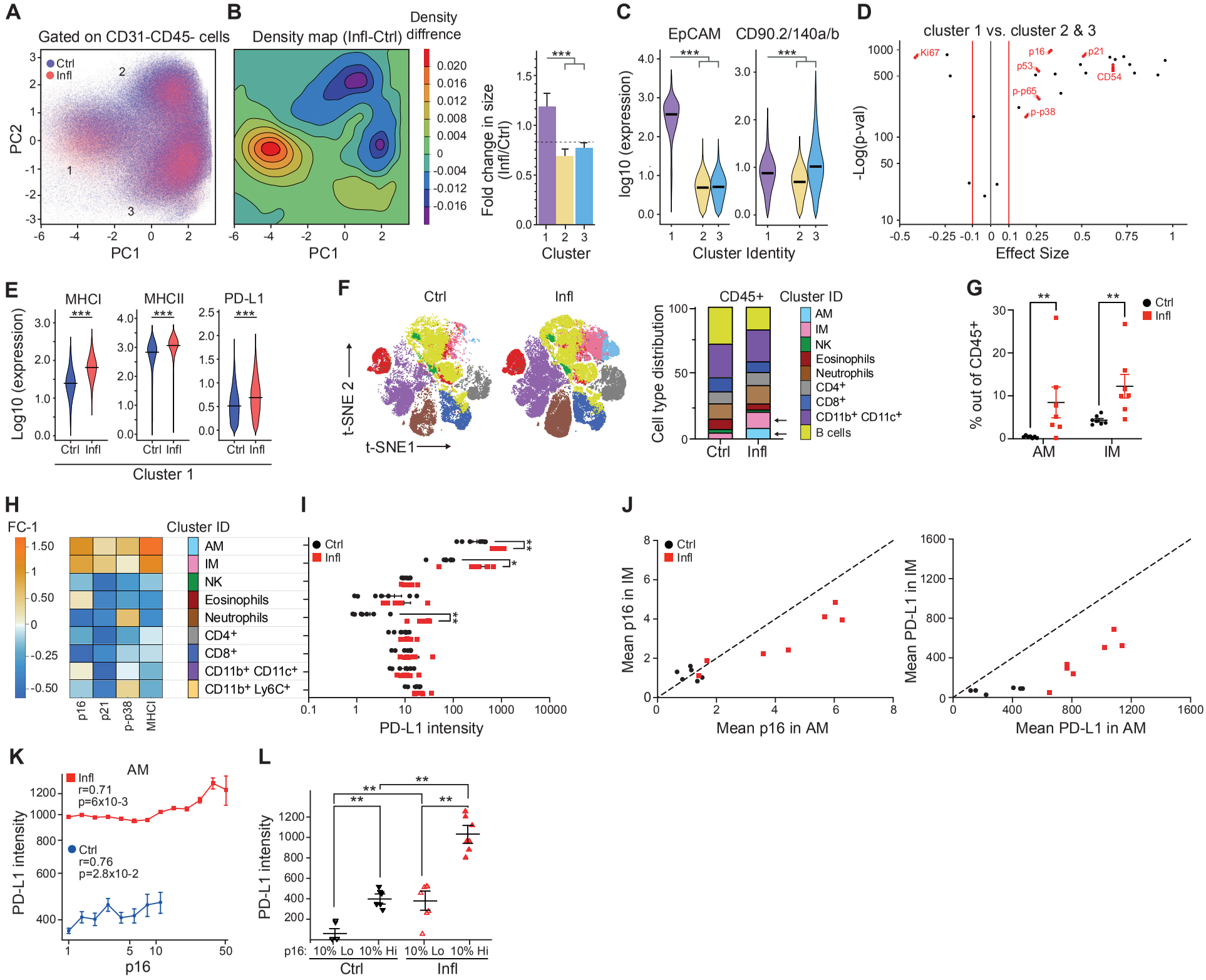
A
Gated on CD31-CD45- cells
Ctrl
Infl
PC2
PC1
B
Density map (Infl-Ctrl)
Density diffrence
0.020
0.016
0.012
0.008
0.004
0
-0.004
-0.012
-0.016
Fold change in size (Infl/Ctrl)
Cluster
C
EpCAM
CD90.2/140a/b
log10 (expression)
Cluster Identity
D
cluster 1 vs. cluster 2 & 3
Ki67
p16
p21
p53
CD54
p-p65
p-p38
-Log(p-val)
Effect Size
E
MHCI
MHCII
PD-L1
Log10 (expression)
Ctrl
Infl
Cluster 1
F
Ctrl
Infl
t-SNE 2
t-SNE1
CD45+
Cluster ID
Cell type distribution
AM
IM
NK
Eosinophils
Neutrophils
CD4+
CD8+
CD11b+ CD11c+
B cells
G
% out of CD45+
AM
IM
H
FC-1
Cluster ID
CD11b+ Ly6C+
p16
p21
p-p38
MHCI
I
PD-L1 intensity
J
Mean p16 in IM
Mean p16 in AM
Mean PD-L1 in IM
Mean PD-L1 in AM
K
AM
r=0.71
p=6x10-3
r=0.76
p=2.8x10-2
p16
L
p16: 10% Lo 10% Hi 10% Lo 10% Hi

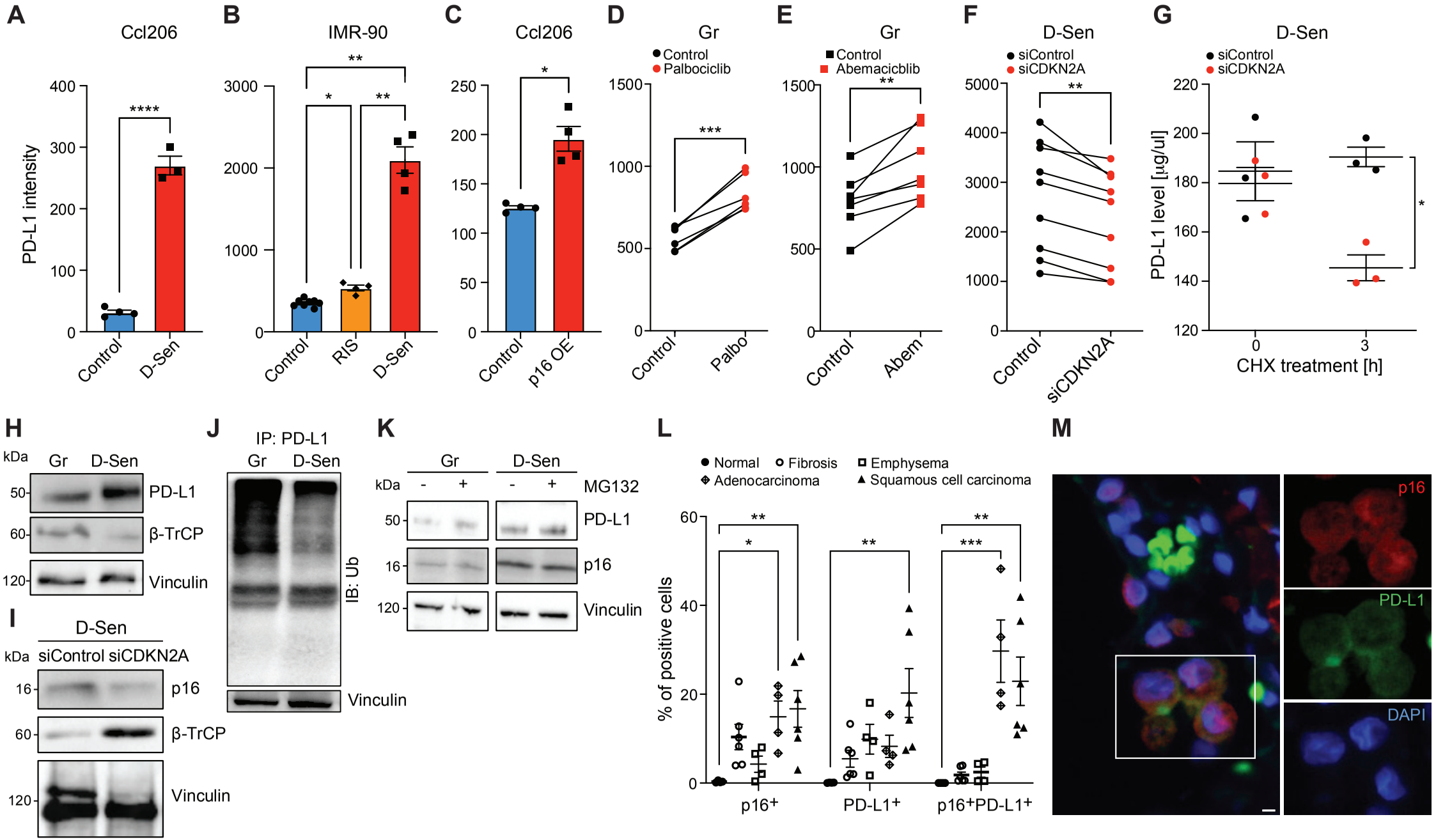
A
Ccl206
PD-L1 intensity
Control
D-Sen
B
IMR-90
Control
RIS
D-Sen
C
Ccl206
Control
p16 OE
D
Gr
Control
Palbociclib
Control
Palbo
E
Gr
Control
Abemacicblib
Control
Abem
F
D-Sen
siControl
siCDKN2A
Control
siCDKN2A
G
D-Sen
siControl
siCDKN2A
PD-L1 level [µg/ul]
CHX treatment [h]
H
kDa
Gr
D-Sen
PD-L1
β-TrCP
Vinculin
I
D-Sen
siControl
siCDKN2A
p16
β-TrCP
Vinculin
J
IP: PD-L1
Gr
D-Sen
IB: Ub
Vinculin
K
Gr
D-Sen
MG132
PD-L1
p16
Vinculin
L
Normal
Fibrosis
Emphysema
Adenocarcinoma
Squamous cell carcinoma
% of positive cells
p16+
PD-L1+
p16+PD-L1+
M
p16
PD-L1
DAPI

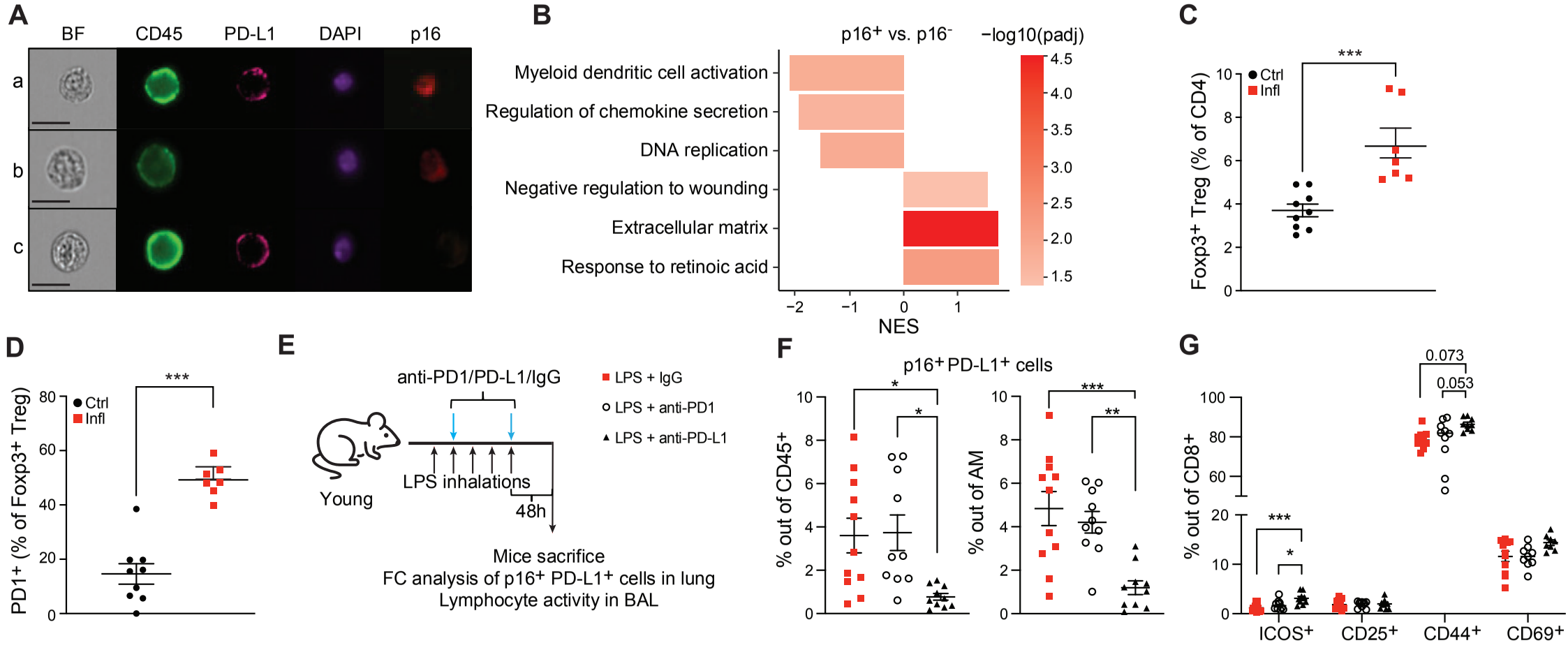
A
BF
CD45
PD-L1
DAPI
p16
a
b
c
B
p16+ vs. p16-
−log10(padj)
Myeloid dendritic cell activation
Regulation of chemokine secretion
DNA replication
Negative regulation to wounding
Extracellular matrix
Response to retinoic acid
NES
C
Ctrl
Infl
Foxp3+ Treg (% of CD4)
D
PD1+ (% of Foxp3+ Treg)
E
anti-PD1/PD-L1/IgG
LPS + IgG
LPS + anti-PD1
LPS + anti-PD-L1
Young
LPS inhalations
48h
Mice sacrifice
FC analysis of p16+ PD-L1+ cells in lung
Lymphocyte activity in BAL
F
p16+ PD-L1+ cells
% out of CD45+
% out of AM
G
% out of CD8+
ICOS+
CD25+
CD44+
CD69+
0.073
0.053

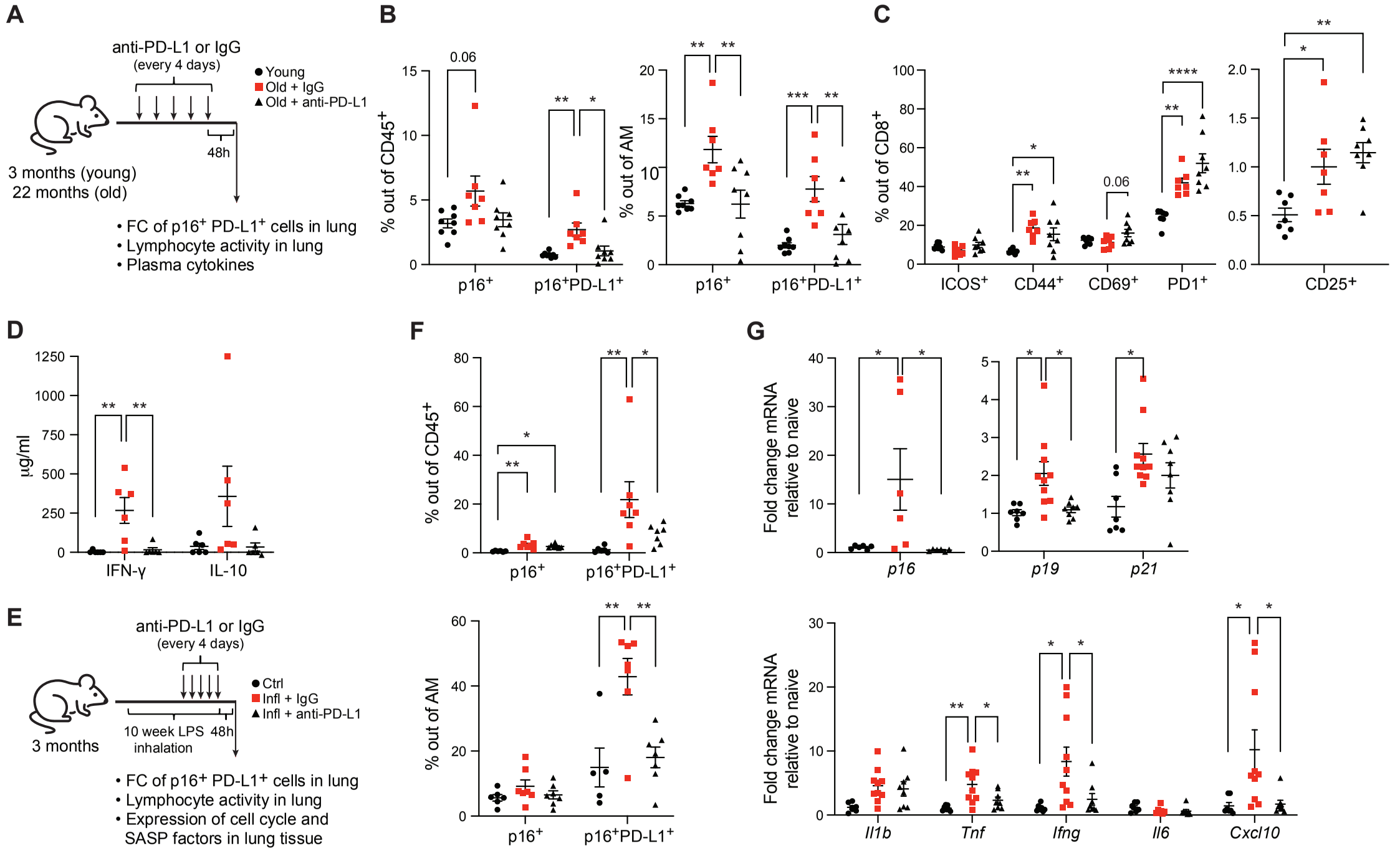
A
anti-PD-L1 or IgG
(every 4 days)
Young
Old + IgG
Old + anti-PD-L1
48h
3 months (young)
22 months (old)
• FC of p16+ PD-L1+ cells in lung
• Lymphocyte activity in lung
• Plasma cytokines
B
% out of CD45+
% out of AM
0.06
p16+
p16+PD-L1+
C
% out of CD8+
ICOS+
CD44+
CD69+
PD1+
CD25+
D
µg/ml
IFN-γ
IL-10
E
anti-PD-L1 or IgG
(every 4 days)
Ctrl
Infl + IgG
Infl + anti-PD-L1
3 months
10 week LPS inhalation
48h
• FC of p16+ PD-L1+ cells in lung
• Lymphocyte activity in lung
• Expression of cell cycle and SASP factors in lung tissue
F
% out of CD45+
% out of AM
p16+
p16+PD-L1+
G
Fold change mRNA relative to naive
p16
p19
p21
Il1b
Tnf
Ifng
Il6
Cxcl10

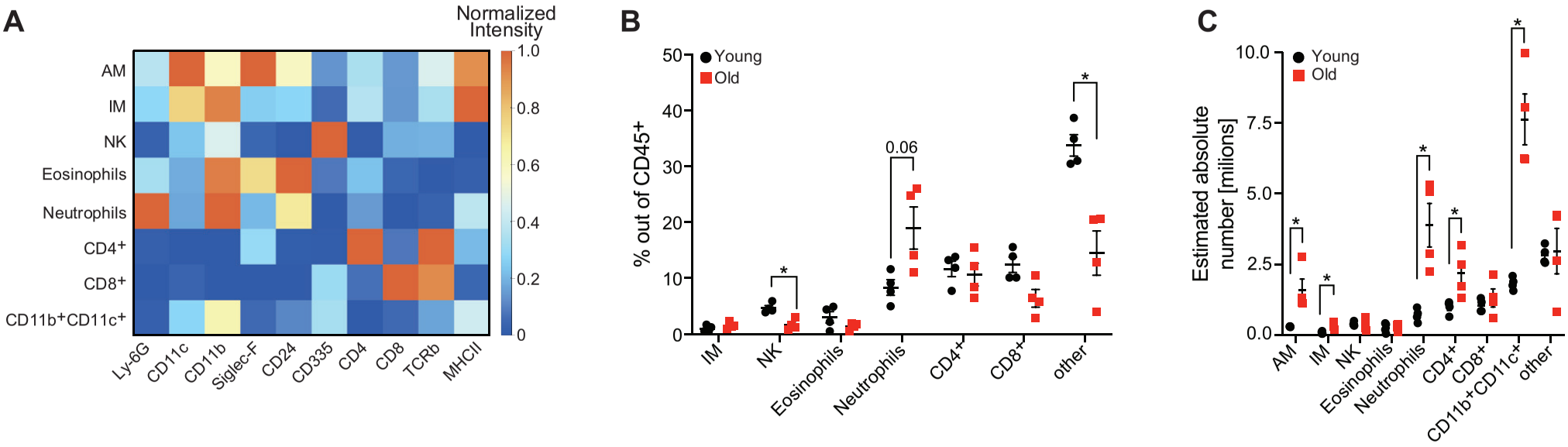
A
Normalized Intensity
1.0
0.8
0.6
0.4
0.2
0
AM
IM
NK
Eosinophils
Neutrophils
CD4+
CD8+
CD11b+CD11c+
Ly-6G
CD11c
CD11b
Siglec-F
CD24
CD335
CD4
CD8
TCRb
MHCII
B
Young
Old
% out of CD45+
50
40
30
20
10
0
0.06
*
IM
NK
Eosinophils
Neutrophils
CD4+
CD8+
other
C
Young
Old
Estimated absolute number [milions]
10.0
7.5
5.0
2.5
0.0
*
AM
IM
NK
Eosinophils
Neutrophils
CD4+
CD8+
CD11b+CD11c+
other

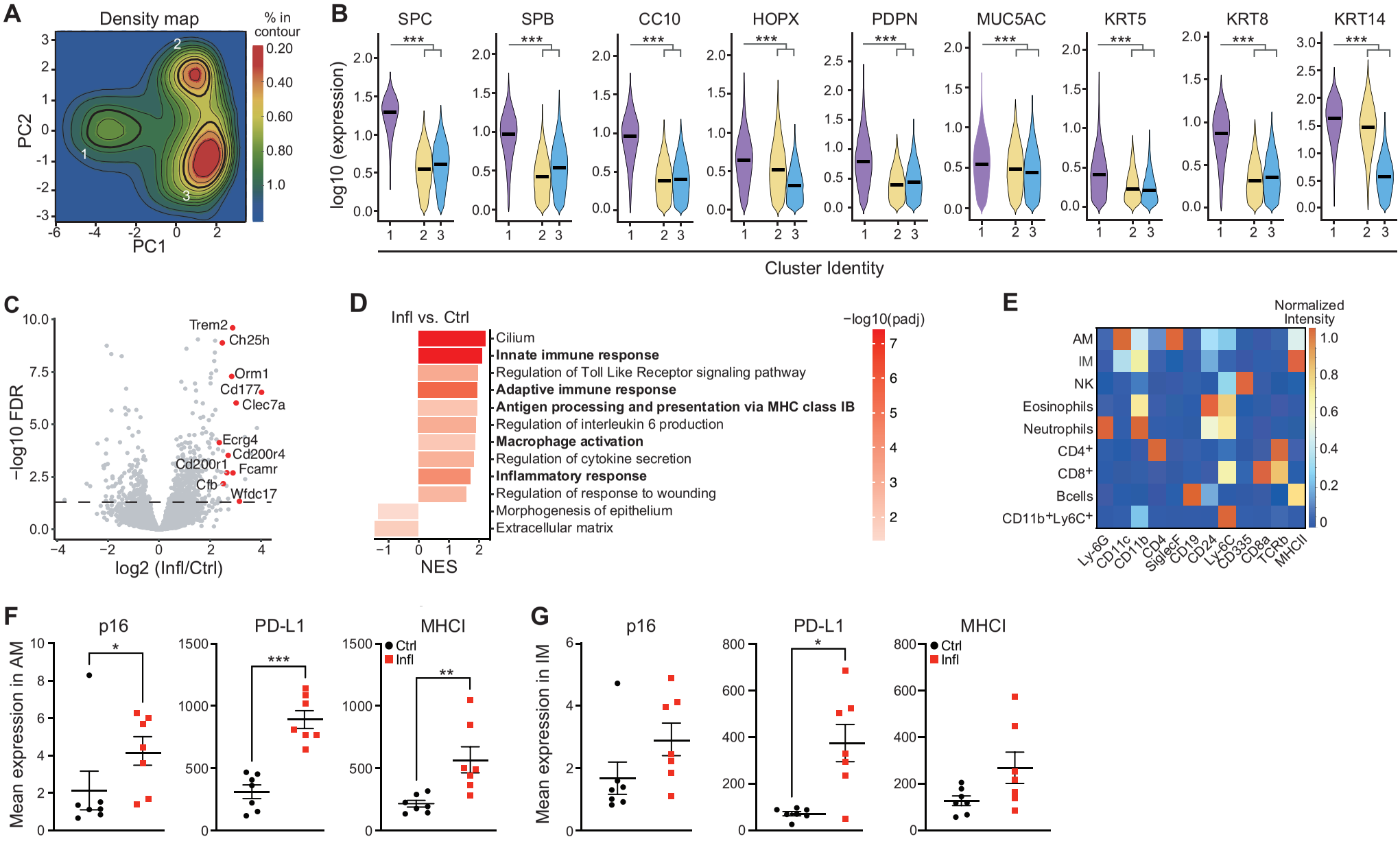
A
Density map
% in contour
0.20
0.40
0.60
0.80
1.0
PC2
PC1
1
2
3
B
SPC
SPB
CC10
HOPX
PDPN
MUC5AC
KRT5
KRT8
KRT14
***
log10 (expression)
Cluster Identity
C
Trem2
Ch25h
Orm1
Cd177
Clec7a
Ecrg4
Cd200r4
Cd200r1
Fcamr
Cfb
Wfdc17
−log10 FDR
log2 (Infl/Ctrl)
D
Infl vs. Ctrl
Cilium
Innate immune response
Regulation of Toll Like Receptor signaling pathway
Adaptive immune response
Antigen processing and presentation via MHC class IB
Regulation of interleukin 6 production
Macrophage activation
Regulation of cytokine secretion
Inflammatory response
Regulation of response to wounding
Morphogenesis of epithelium
Extracellular matrix
NES
−log10(padj)
E
Normalized Intensity
AM
IM
NK
Eosinophils
Neutrophils
CD4+
CD8+
Bcells
CD11b+Ly6C+
Ly-6G
CD11c
CD11b
CD4
SiglecF
CD19
CD24
Ly-6C
CD335
CD8a
TCRb
MHCII
F
p16
PD-L1
MHCI
Ctrl
Infl
Mean expression in AM
G
Mean expression in IM

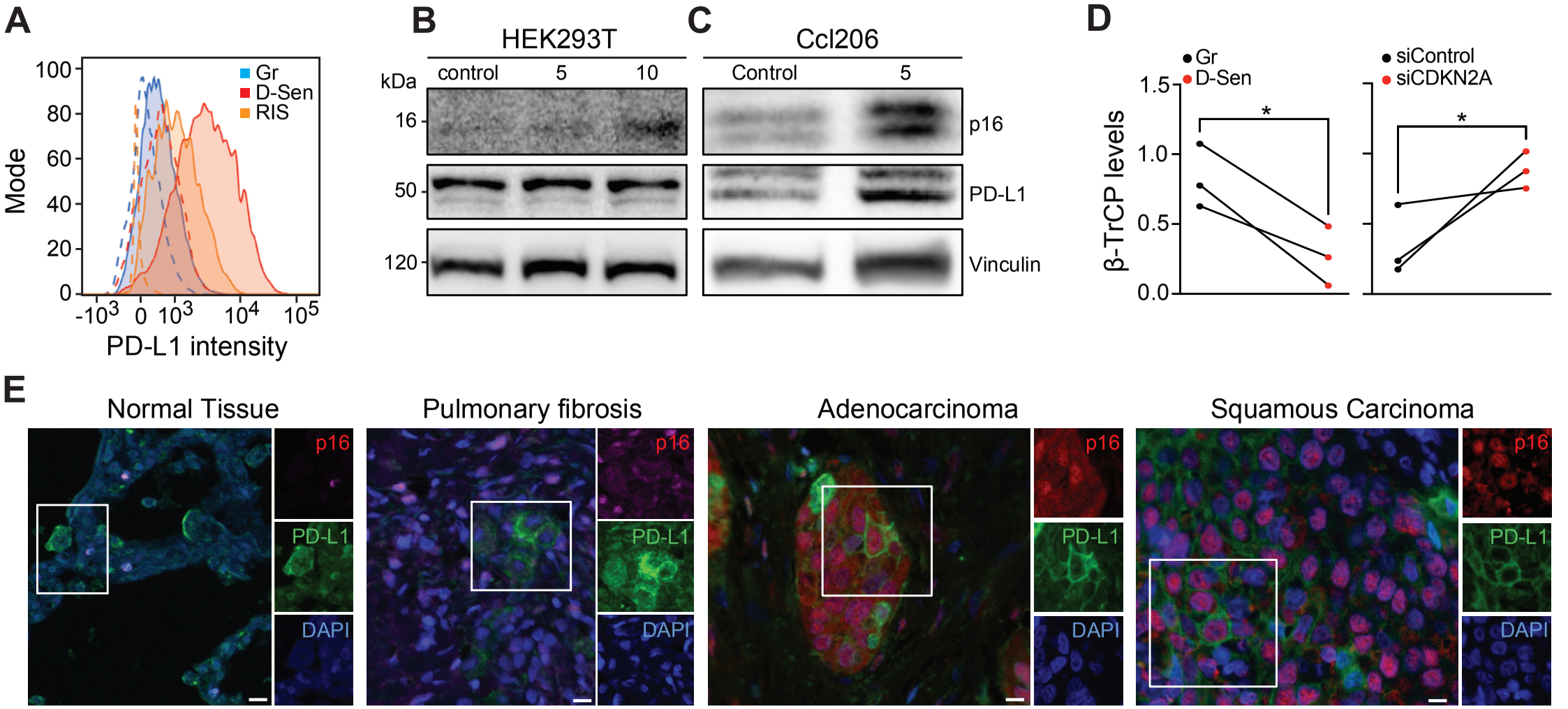
A
Mode
PD-L1 intensity
Gr
D-Sen
RIS
B
HEK293T
kDa
control
5
10
16
50
120
C
Ccl206
Control
5
p16
PD-L1
Vinculin
D
β-TrCP levels
Gr
D-Sen
siControl
siCDKN2A
E
Normal Tissue
Pulmonary fibrosis
Adenocarcinoma
Squamous Carcinoma
p16
PD-L1
DAPI

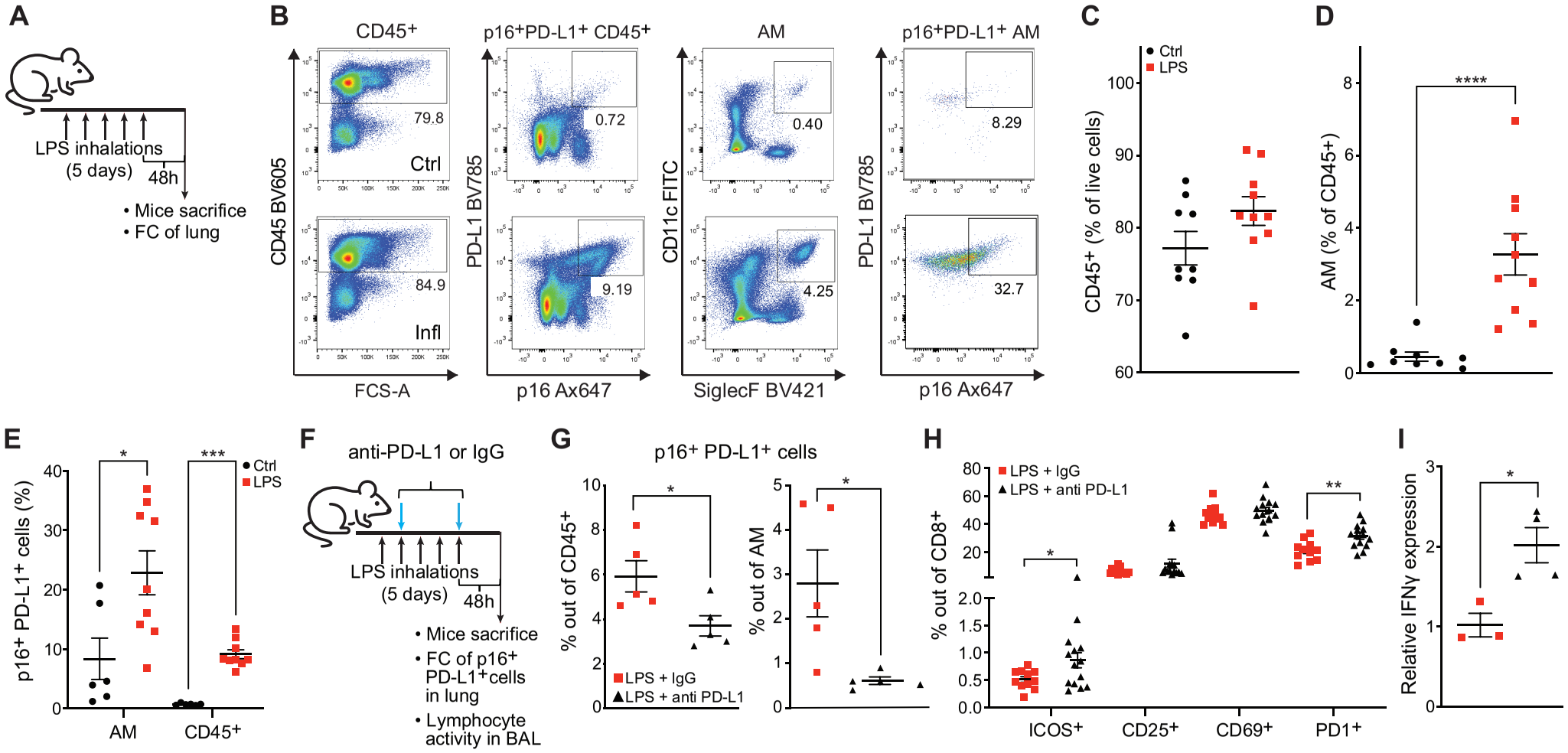
A
LPS inhalations
(5 days)
48h
• Mice sacrifice
• FC of lung
B
CD45+
p16+PD-L1+ CD45+
AM
p16+PD-L1+ AM
79.8
Ctrl
84.9
Infl
0.72
9.19
0.40
4.25
8.29
32.7
CD45 BV605
FCS-A
PD-L1 BV785
p16 Ax647
CD11c FITC
SiglecF BV421
C
Ctrl
LPS
CD45+ (% of live cells)
D
****
AM (% of CD45+)
E
p16+ PD-L1+ cells (%)
AM
CD45+
F
anti-PD-L1 or IgG
LPS inhalations
(5 days)
48h
• Mice sacrifice
• FC of p16+ PD-L1+cells in lung
• Lymphocyte activity in BAL
G
p16+ PD-L1+ cells
% out of CD45+
% out of AM
LPS + IgG
LPS + anti PD-L1
H
% out of CD8+
ICOS+
CD25+
CD69+
PD1+
I
Relative IFNγ expression

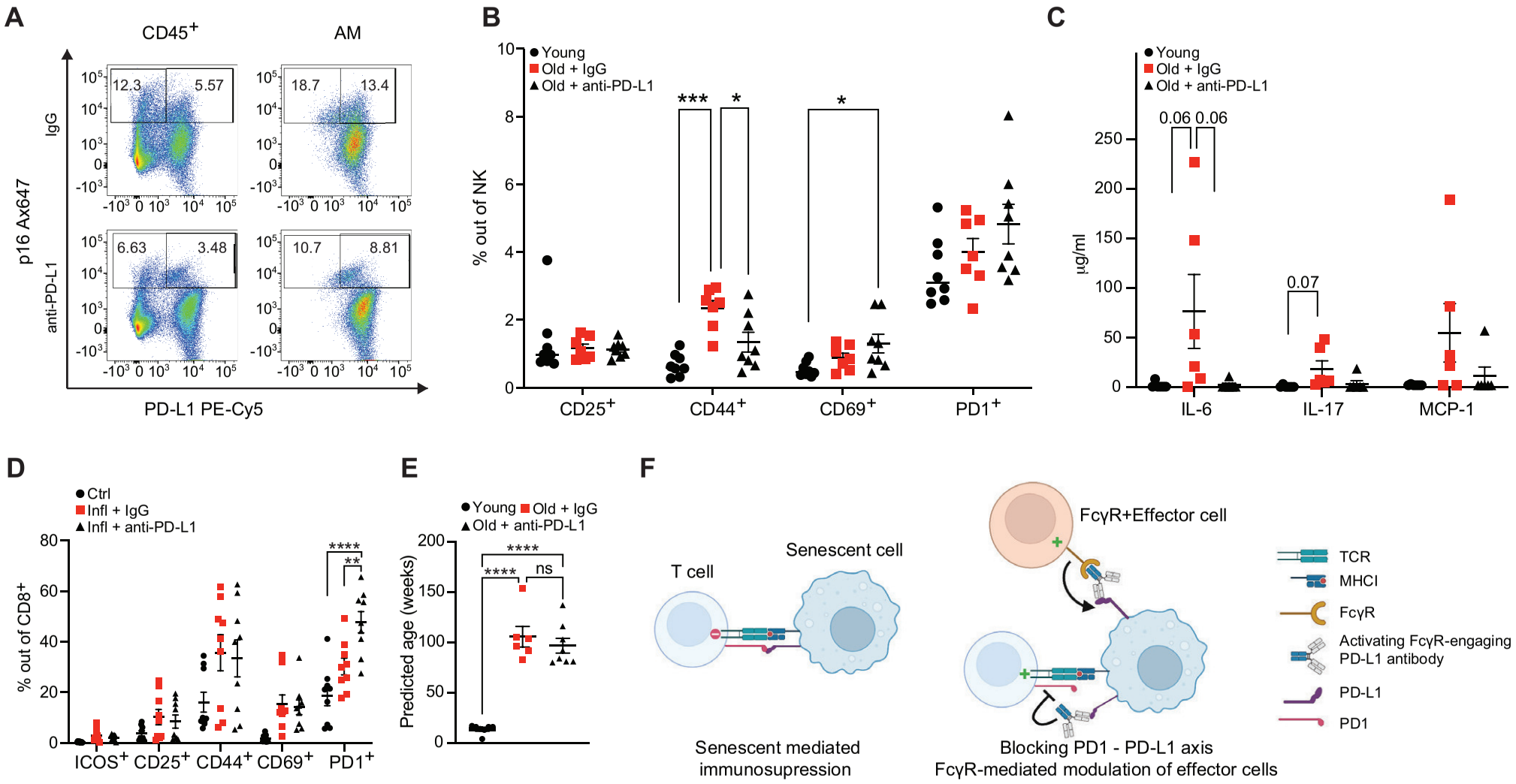
A
CD45+
AM
IgG
anti-PD-L1
p16 Ax647
PD-L1 PE-Cy5
12.3
5.57
18.7
13.4
6.63
3.48
10.7
8.81
B
Young
Old + IgG
Old + anti-PD-L1
% out of NK
***
*
*
CD25+
CD44+
CD69+
PD1+
C
Young
Old + IgG
Old + anti-PD-L1
µg/ml
0.06 0.06
0.07
IL-6
IL-17
MCP-1
D
Ctrl
Infl + IgG
Infl + anti-PD-L1
% out of CD8+
****
**
ICOS+ CD25+ CD44+ CD69+ PD1+
E
Young
Old + IgG
Old + anti-PD-L1
Predicted age (weeks)
****
****
ns
F
T cell
Senescent cell
Senescent mediated immunosupression
FcγR+Effector cell
Blocking PD1 - PD-L1 axis
FcγR-mediated modulation of effector cells
TCR
MHCI
FcγR
Activating FcγR-engaging PD-L1 antibody
PD-L1
PD1